NOVEL FABRICATION OF FLEXIBLE MICROELECTRODES WITH MACROPOROUS PLATINUM FILM USING LATEX POLYSTYRENE SPHERE TEMPLATE

by

Nominerdene Oyunerdene

B.S., The University of Washington, Seattle, 2011

A THESIS SUBMITTED IN PARTIAL FULFILLMENT OF

THE REQUIREMENTS FOR THE DEGREE OF

MASTER OF APPLIED SCIENCE

in

THE FACULTY OF GRADUATE AND POSTDOCTORAL STUDIES

(Electrical and Computer Engineering)

THE UNIVERSITY OF BRITISH COLUMBIA

(Vancouver)

October 2014

Abstract

With great strides in neuroscience that have been made in the past decade, further understandings of complex neural systems require extensive neural information from chronic implantation of biocompatible neural devices. Polyimide-based flexible microelectrode arrays were one of the earlier biocompatible neural devices due to its mechanical impedance matching with brain tissue.

In this work, we propose to incorporate non-conventional laser ablation method for fabrication of flexible biocompatible microelectrodes. We also present a novel approach to modifying flexible microelectrodes with macroporous platinum film using latex polystyrene sphere template. Maskless laser ablation was used to pattern the electrode, and probe definition as well creating the contact openings of flexible polyimide electrodes. Laser ablation is a non-photolithographic method which does not require conventional cleanroom environment and is ideal for rapid prototyping of devices.

An ordered polystyrene bead template was deposited by simple pipetting of bead solution over gold contact openings and evaporating in ambient room setting. Pulsed-potentiostatic mode electrochemical deposition of platinum through the polystyrene bead template resulted in increase in effective surface area of electrodes. The impedance of the platinum modified electrodes increased by two orders of magnitude compared to unmodified electrodes. Synergetic modification of microelectrodes with macroporous platinum film and polymer-brush coating can lead to fabrication of highly biocompatible microelectrode with low impedance characteristics.

Preface

The polymer brush coating process stated in Section 2.2 was carried out by Dr. Madhab Bajgai in Dr. Jayanchandran's lab in Department of Pathology at UBC.

Eric Cheng, M.A.Sc. Candidate, UBC ECE, carried out the inkjet printing of polystyrene solution experiment, as described in Section 2.3.1.2 and provided the experimental setup.

The electrochemical deposition of platinum film is collaboration with Professor Dan Bizzotto and his student Isaac Martins from UBC Chemistry Department. Initial electrochemical deposition of platinum was carried together with Isaac Martin but as I become more experienced in electrochemistry, I carried out the bulk of the electrochemistry experiments with minor supervision from Isaac.

All other work including complex impedance characterization using the impedance analyzer, LEXT image analysis and thickness measurements, fabrication of substrates for experiments, laser ablation of all substrates and polystyrene bead template deposition was carried out by me.

Table of Contents

List of Tables

List of Figures

Acknowledgements

I would like to thank my supervisor Karen Cheung, who has provided me with the opportunity to pursue this great endeavor. I have grown a lot as a person during my studies here and would not be possible without your help and guidance. I would also like to thank my lab mates at the BioMEMS lab for their support and company.

I want to thank Professor Dan Bizzotto and his student Isaac Martins for helping me with the electrochemistry setup and guidance. I wish to thank Madhab Bajgai for his work on the polymer brush coating. I also want to thank Jim, Mario and Alina at the ANF facilities for their tremendous help.

I would not be the person I am today without so many great friends and people who have been instrumental to my path in life. I just want say that I say it without saying it. The dearest of them all is my family.

Dedication

To my family.

Chapter 1: Introduction

Neural interfaces have important clinical applications and are also important in advancements in learning more about the brain. Commercially available neural prosthetics include deep brain stimulators and cochlear implants.

Microelectrodes are implemented using various materials and methods, ranging from microwire arrays [1], which continue to be used today, to microfabricated silicon, metal [2], ceramic [3], and polymer-based arrays [4-7]. The initial miniaturized, batch-fabricated microelectrode arrays were silicon based devices, the fabrication methods and material choices benefiting from onset of microfabrication techniques used for early computer chip technology [8]. Material choice and novel fabrication advancements in micromachining allowed the creation of flexible, polymer-based microelectrode arrays. Flexible, polymer-based microelectrodes allow for decreased device-tissue interaction which contributes to improvement in biocompatibility of microelectrodes. Recently, researchers have focused on improving the long-term biocompatibility of microelectrodes as it has been shown that performance of microelectrodes degrade after a period of 4 weeks due to the natural tissue response [9]. Polymer brush coated polyimide insulators have decreased tissue-response activity on the polyimide surface while the electrode impedance increased due to the coating. The ideal electrode has high signal-to-noise ratio which is an effect of having minimum impedance. The impedance of the electrode can be decreased by modifying the surface of the electrode contact opening with micro/nano features that effectively increase the total surface area of the electrode while maintaining the same geometric cross-sectional area [10].

This work incorporates novel fabrication methods to existing flexible biocompatible microelectrodes and improves the electrical characteristics of the electrodes through novel electrochemical deposition of macroporous platinum film using macroporous polystyrene sphere template. Maskless laser ablation is used to pattern the electrode, and probe definition as well creating the contact openings. Laser ablation is a non-photolithographic method which does not require a cleanroom environment and is ideal for rapid prototyping of devices. A novel approach to achieve macroporous platinum using simple pipetting of polystyrene sphere bead template and electrochemical deposition can be done in a simple laboratory environment. The impedance of the platinum modified electrodes is compared to unmodified electrodes. The change in impedance is a result of increased electrochemically active surface area with respect to flat, unmodified electrodes.

1.1 Motivation

Traumatic injuries and crippling diseases can disrupt the natural flow of electrical information in the human central nervous system (CNS) sensory modules, and motor tissue. Neuroprosthetic devices, which aim to re-wire the disruption, can be used to treat the specific injury or disease in patients and significantly improve their way of living. Neuroprosthetic devices work on the basis that neural probes can extract motor intent information from summed electrical activities of cortical neurons in the region of interest in the central nervous system, and using the derived information to control a prosthetic device or re-wiring to another module of the CNS. Existing neuroprosthetic devices include deep brain stimulators (DBS) [11], cochlear implants [12],

retinal prosthetics [13], and neural recording of large-scale cortical activity in rhesus monkeys to help neuroscientists' gain deeper understanding of the brain [14].

Deep brain stimulators have greatly helped patients suffering from Parkinson's disease (PD) and essential tremor (ET) [15]. DBS applies high frequency electrical signals using cortical electrodes to regions of the CNS that govern movement. DBS used in different regions of the CNS have been shown to mitigate chronic pain as well [11]. Cochlear implants and retinal prosthetics function by transducing input from microphone and camera to electrical signals which are then applied to auditory nerves and retinal ganglion cells, respectively, using implanted electrodes [13].

Simultaneous wireless large-scale recording of close to 500 cortical neurons, distributed across multiple regions of the brain, was achieved using surgically implanted multielectrode system [14]. The researchers were able to record over a period as long as 5 years in freely moving primates. Expansion of the criterion set by such an experiment can lead to a complex neuroprosthetic such as a brain-controlled robotic limb.

In future neuroprosthetic devices, electrodes are expected to be biocompatible and minimally invasive to the implanted region of CNS or PNS. Advances in fabrication technology allows for novel approach to fabricating biocompatible microelectrodes that can record from multiple sites at a given time.

1.2 Neurophysiology

Information between neurons is transmitted through the axon-dendrite connection. A neuron has a single output node, the axon, which sends information as an action potential to an input node of another neuron, called the dendrite. A neuron will have multiple dendrites which integrate input from multiple neurons until a threshold potential is reached, at which point the neuron will fire an action potential to another neuron through the axon [16]. Action potential between neurons are generated and propagated by ionic charge carriers within an electrolyte such as potassium (K^+) and sodium (Na^+) [10].

1.3 Neural electrodes

The first microelectrodes were in form of sharpened microwires, implanted in live animals [17]. An insulated tungsten wire with an exposed tip was used to record from single neurons over a period of a week. Microwires are still widely used in current neurophysiological studies. In the study by Nicocelis et al [1], multichannels of microwires numbering up to 1792 were implanted in live behaving rhesus monkeys to make large-scale recordings from multiple regions of the brain. Advances in understandings of the neural systems have progressed to a point where simultaneous recording from large-scale neuron population is required to drive bleeding edge brain-machine interfaces [18].

1.3.1 Silicon-based electrodes

Advent of silicon-based microelectronic fabrication methods has made it possible to fabricate multielectrode arrays (MEAs) capable of simultaneously recording from multiple sites. The advanced silicon fabrication techniques and process allows for well-defined parameters such as

spacing between electrode recording sites and sizing of probe lengths as well as integration with on-chip electronics.

One of the first silicon microelectrode systems is known as the “Michigan” array, first developed by Wise et al [19]. The Michigan array is an in-plane electrode -- the electrode is fabricated along the plane of the silicon wafer therefore its length is limited by the size of the silicon wafer used. Multiple recording sites can be positioned along each shank and is quite useful for deciphering information from neurons from multiple cortex sublevels. The MEA can be fabricated with integrated CMOS circuitry on board. A simplified process flow is shown Figure 1.

First, deep boron diffusion step is used to define the substrate shape. Bottom dielectric layer is deposited, followed by deposition and patterning of the conductor layer. Next, the top dielectric layer is deposited and electrode sites for the titanium/iridium layer are defined using a lift-off process. The probe is then released from the substrate by dissolving the wafer using an ethylene diamine pyrocatechol (EDP) etch.

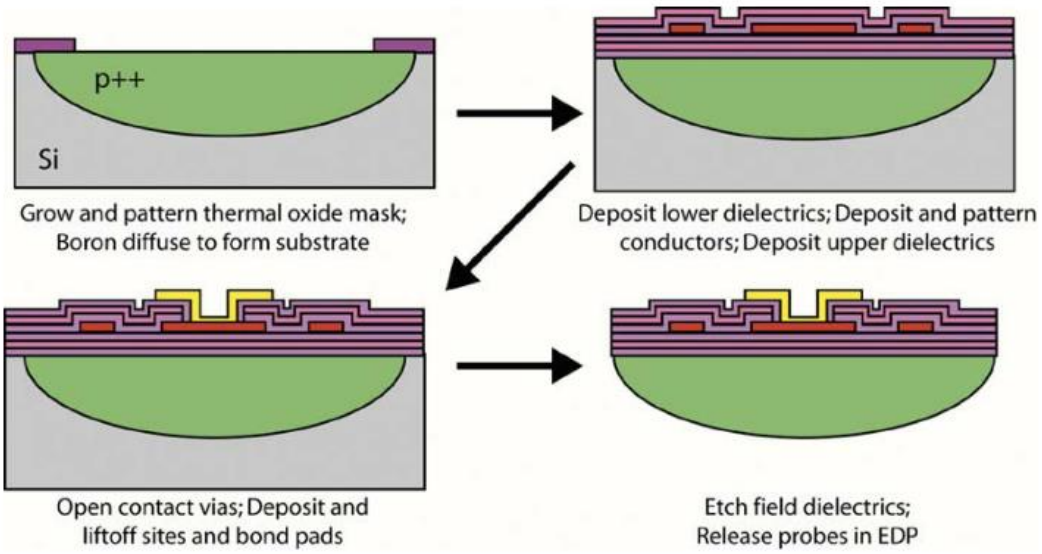

Figure 1. Basic flow diagram for fabrication of a passive Michigan array [19]

1.3.2 Polymer-based electrodes

Tissue response to inflammation at the electrode implant site caused by micromotion between the stiff electrode and brain tissue can result in glial scars passivating the electrode. Glial scars are a natural response to inflammation in physiological systems that encapsulate the implanted electrodes, rendering them useless [21]. Silicon has a Young's modulus of 170GPa, while brain tissue has a value of 3 kPa, therefore a small relative motion by a live behaving animal under a neuroscience can result in inflammation at the implant site. A flexible MEA can minimize the amount of inflammation that can occur due to mechanical mismatch between the implanted electrode and brain tissue due to the ability to conform more to the micromotion.

Polyimide has a Young's modulus of 3 GPa while providing good insulation resistance and dielectric strength. Polyimide-based MEA can also be fabricated using existing

photolithographic processes. Flexible MEAs can be implemented using polyimide as an insulating and encapsulating material [22]. A simplified process flow of a polyimide-based flexible MEA is shown in Figure 2.

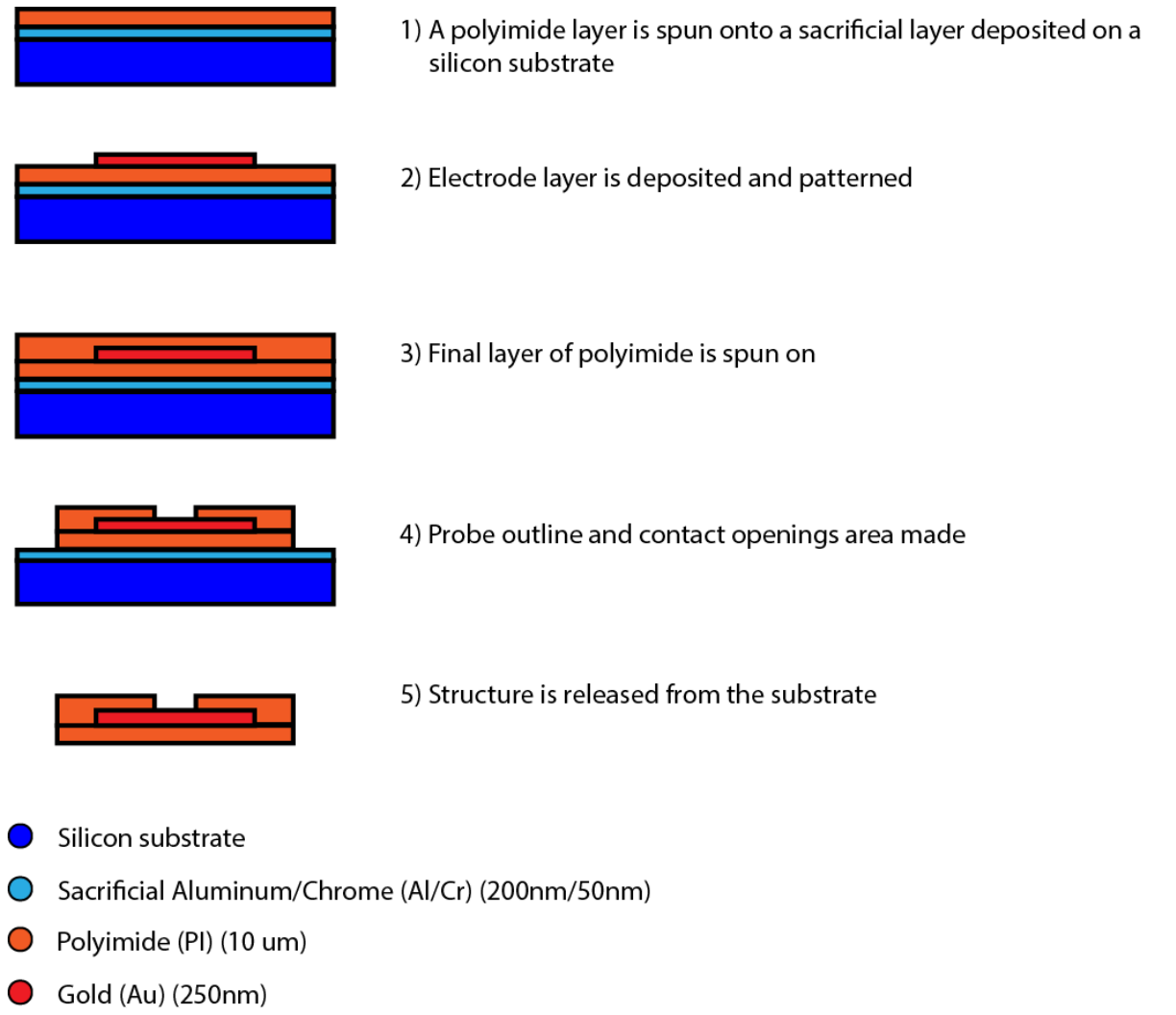

Figure 2. Process flow for polyimide-based MEA. 1) Sacrificial aluminum (Al) layer is deposited over a silicon substrate and polyimide is spun onto the Al layer. 2) The metal layer is sputtered on and patterned using reactive ion etching (RIE). 3) Insulating polyimide layer is spun on 4) RIE is used to define probe definition as well as the contact openings. 5) The probe is released from the substrate using anodic dissolution of the artificial layer [20]

1.4 Tissue response to implanted microelectrodes

It is important to investigate the feasibility of MEAs for chronic applications and brain tissue response to the electrode is seen as the important factor in chronic implementation of MEAs.

There are two inter-related responses to electrode-insertion in brain tissue. For the initial response, microglia and astrocyte cells concentrate around the inserted device within hours of initial implantation [20]. Microglia response is related to release of inflammatory molecules such as nitric oxide which induce neuronal cell death and activate astrocytes [21]. The magnitude of initial response is proportional to the cross sectional area of the device [23].

For the chronic response, astrocytes accumulate to form a sheath around the device. A sheath of 50-100 um radius around the implanted device is observed after 4 weeks [20]. While the sheath insulates the electrode from the neurons, it has also been shown to increase electrical impedance of the electrode [25]. One possible source of signal degradation is believed to be that of continued reaction of microglia and astrocytes incur neuronal cell death around the electrode. No increase in density of neurons near the sheath zone was observed which indicate that neurons were not pushed away from the implant site [21].

1.4.1 Surface coating to increase biocompatibility

One of the strategies to reduce inflammatory response at the implant site is through surface modification of the implanted electrodes with materials that reduce glial response at the site while promoting neuron growth. Modification with specific bioactive peptides has been shown to selectively reduce glial cell activity at the electrode site while promoting neuronal growth [25].

Modification with polyethylene glycol (PEG) can reduce overall tissue response, protein adsorption and cell adhesion, at the electrode site. It is believed that protein adsorption at the electrode site is initial response to implanted devices that is followed by cell adhesion and the inflammatory response [23]. Recently, multi-functional bioactive polymer brush coatings have been shown to be good surface modification that can increase desired response at the electrode surface [26]. Polymer brush modifications do not change the bulk characteristic of the electrode and the polymer properties can be tailored on the surface in a controlled process [26].

1.5 Electrode model

The charger carriers in electrodes consist of electrons and holes, as opposed to ionic charger carriers mentioned in Section 1.2. Therefore, the bio-electrode interface transduces information between the electrode and neurons. When a metal is placed in ionic solution at zero bias, a space charge layer builds up at the electrode/solution layer due to the oxidation of the metal. Eventually, equilibrium is reached between the oxidation and reduction reactions. A hydration sheath of oriented water molecules form what is called the inner Helmholtz layer while another layer of hydrated ions from the second outer Helmholtz layer [10]. The metal-tissue interface is therefore a capacitive-resistive interface. A simplified equivalent circuit model of an electrode-tissue interface is shown in Figure 3.

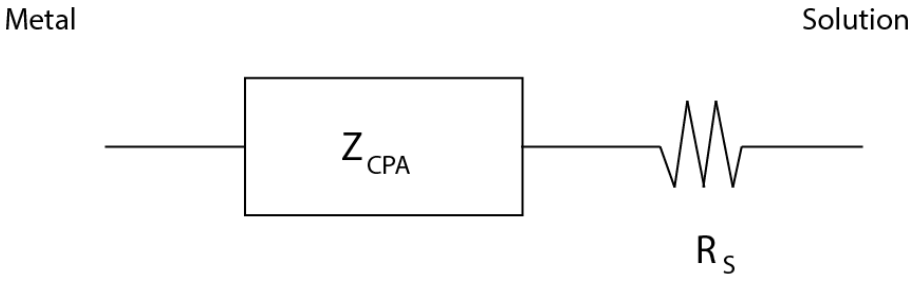

Figure 3. Equivalent circuit model of the electrode-tissue interface

Interface capacitance, Z_{CPA} is in series with solution resistance, R_S. The interface capacitance is the combination of the Helmholtz layer capacitance and the diffuse layer capacitance. The diffuse layer is a space charge layer outside the Helmholtz layer in the bulk solution. The interface capacitance can be described using the parallel-plate capacitor equation [10]:

$$\boldsymbol{C = \frac{\varepsilon_0 \varepsilon_r A}{d}} \tag{1}$$

Where ε_0 is the dielectric permittivity of free space, ε_r is the relative dielectric permittivity of the medium between the two plates, A is the surface area of the plates, and d is the distance between the plates. Therefore, the interface capacitance of the electrode is proportional to the surface area of the electrode. The solution resistance for a square electrode is defined by the following equation:

$$\boldsymbol{R_s = \frac{\rho \ln(4)}{\pi l}} \tag{2}$$

where ρ is the conductivity of the solution and l is the length of one side of the electrode. The simplified circuit model for the electrode has the following RC time constant which would determine the cut-off frequency of the circuit:

$$\tau = R_s C \tag{3}$$

The cut-off frequency would also change according to the change in area of the electrode since the resistive parameter R_S is not dependent on the surface area of the electrode and would remain constant while the interface capacitance changes with respect to surface area. The complex impedance of the circuit is as follows:

$$Z = R_S - \frac{j}{\omega C} \tag{4}$$

The capacitive element of the circuit dominates at lower frequencies while only the resistive element is observed at higher frequencies. Increasing the surface area of the electrode would result in a lower impedance electrode as the capacitance increases and the cut-off frequency increase with surface area modifications.

1.5.1 Increasing surface area through deposition of metal film using macroporous bead template

Previous methods of increasing effective electrode area in order to decrease electrode impedance include electrodeposition of platinum black [26]. However, platinum black can have poor adhesion to the electrode surface. For iridium electrodes, oxidation (activation) can increase the surface roughness [27]. More recently, carbon nanotubes have been grown on electrodes [28] and conducting polymer nanotube coatings [29] have also been used. Our goal in developing templated deposition of nanostructures on the electrodes was to achieve simple, reproducible electrode modification.

A novel method of increasing effective surface area of metal films is by electrochemical deposition (electroplating) of metal through a macroporous latex sphere template [30, 31]. Highly ordered, or single crystalline bead template (Fig. 1 [30]) is achieved by slowly evaporating 500 or 750 nm diameter polystyrene bead solution diluted in water to 0.5 wt % on a 1 cm diameter flat gold surface in a controlled humidity environment over few days. This step is followed by electrochemical deposition of platinum through the template using a common 3-electrode electrochemistry setup. No re-suspension of the latex spheres is believed to occur during deposition of platinum and the spheres are dissolved in toluene solution overnight. The

electrochemically active surface area of the electrode surface is increased due to addition of surface area of the hollow platinum film compared to a flat, non-modified gold surface [31].

1.6 Non-photolithographic mask transfer

Patterning of metal and polymers layers uses a common method of photolithography. The photolithographic process uses masks to define photosensitive mask layers such as photoresist through an optical exposure system. The masking layer is used to define metal patterns on a substrate or insulating layers such as polyimide [20].

Laser ablation is a method that can selectively remove materials from a substrate such as polyimide or gold [33-35]. Laser ablation removes materials in either a photo- or thermo-ablative process. Photo-ablation process usually employs shorter wavelength (~ 300 nm) to break the chemical bonds in the surface layer of the material [36]. With longer wavelength laser ablations, thermal-ablation process occurs. The laser pulse in thermal-ablation causes vibrational excitation at the surface of the material [34]. Ionization at the surface of material results from electromagnetic wave packet exciting the bound electrons and ablation of the material occurs as a result of avalanche ionization. Photo-ablation is the preferred method over thermal-ablation due to minimal thermal damage such as micro-cracks as well as minimal removal of material outside the beam spot [35]. Gold is 40% absorbing at 532 nm and 45% absorbing at 355 nm [36].

Laser ablation-based lithography provides several advantages over conventional photolithographic processes: non-contact, maskless removal of wide range of materials, no solvent chemicals are used in ablation process and rapid prototyping of devices is possible.

However, it is a serial process (i.e. low throughput) and thermal damage can occur if the removal process is thermal in nature. Laser ablation can also be performed in an ambient lab environment whereas conventional photolithography is usually carried out in a cleanroom environment.

1.7 Summary and Objectives

This work incorporates novel fabrication methods to existing flexible biocompatible microelectrodes and improves the electrical characteristics of the electrodes through novel electrochemical deposition of macroporous platinum film using macroporous polystyrene sphere template. Maskless laser ablation is used to pattern the electrode, and probe definition as well creating the contact openings. Laser ablation is a non-photolithographic method which does not require a cleanroom environment and is ideal for rapid prototyping of devices. A novel approach to achieve macroporous platinum using simple pipetting of polystyrene sphere bead template and electrochemical deposition can be done in a simple laboratory environment. The impedance of the platinum modified electrodes is compared to unmodified electrodes. The change in impedance is a result of increased electrochemically active surface area with respect to flat, unmodified electrodes.

Chapter 2: Experimental Methods

2.1 Laser ablation

A typical flow diagram for fabrication of a flexible microelectrode array is shown in Fig. 2. Laser ablation can be used to pattern the electrode layer, probe outline and used to create contact openings, as outlined in Figure 4.

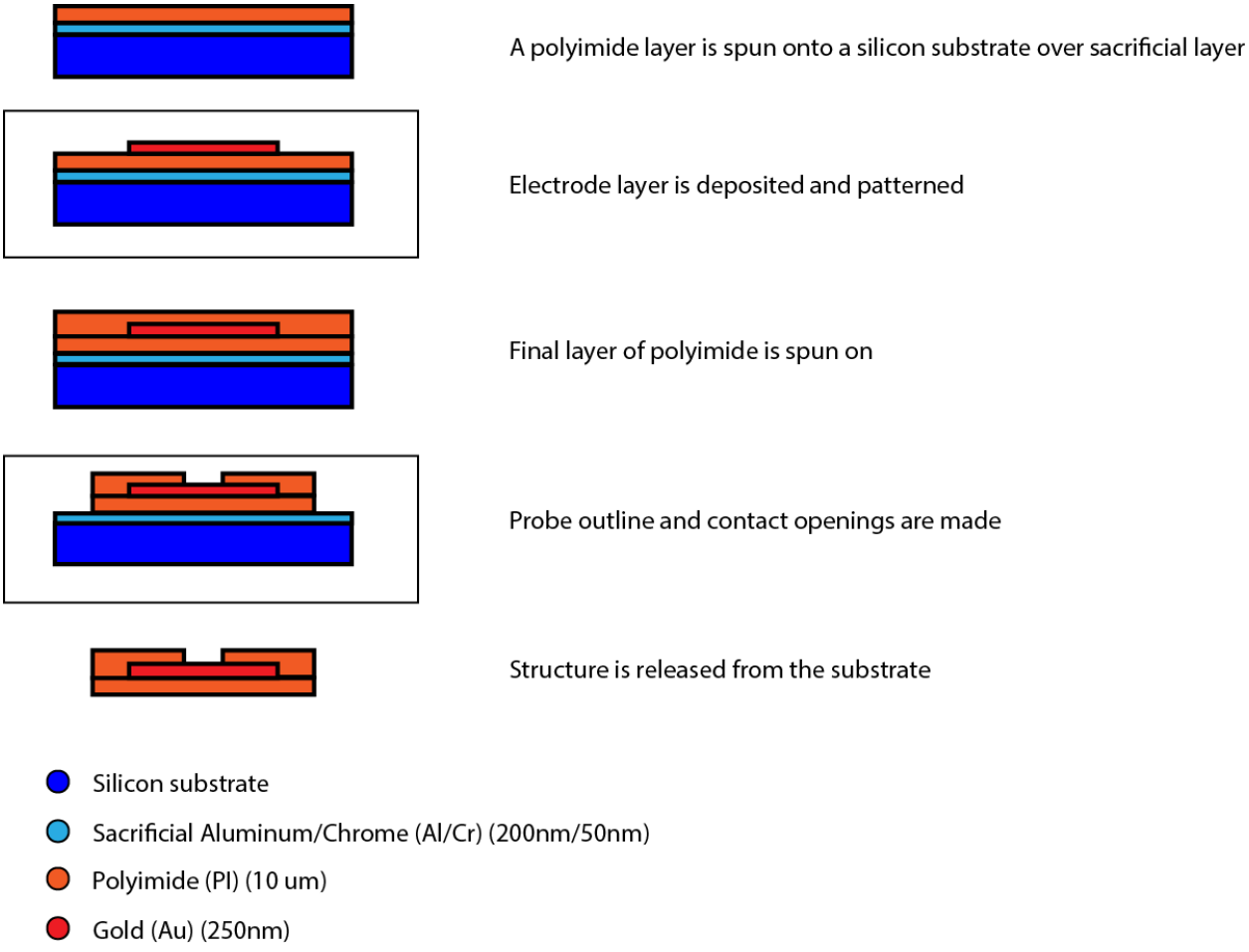

Figure 4. Laser ablation can be used to pattern the electrode layer, probe outline and contact openings as outlined

2.1.1 Laser ablation of gold

For testing of gold/polyimide (Au/PI) substrate laser ablation, 10 µm thick PI (PI-2611, HD Microsystems) is first spun on laboratory glass slide at 1800 rpm for 30 seconds using Laurell WS-400-6NPP-LITE spinner. The PI is soft baked at temperatures of 30° and 60° C for 90 seconds per soft bake temperature. The final curing is done in an oven 300 °C for 30 minutes with a ramp-up rate of 2 ° C/min. The PI thickness is verified using profilometer (Alphastep 200, Tencor). Next, a 50 nm thick adhesion layer of chrome is evaporated followed by evaporation of 250 nm thick gold layer using a DEEWONG-4000 evaporator (ANF facility, UBC). Schematic of the substrate is shown in Figure 5.

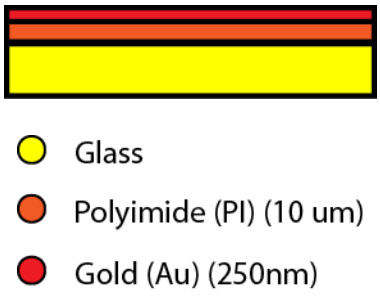

Figure 5. Schematic of polyimide/gold/glass substrate used for ablation of gold

An Nd:YAG laser system is used for the ablation process. The Quiklaze-50 ST2 (ESI, Portland, Oregon) system is capable of two different wavelengths (green: 532 nm, UV3: 355 nm). The system also has two different energy output levels for each wavelength: 0.6 mJ (green HI or UV3 HI) and 0.2 mJ (green LO and UV3 LO). The software system can set the output of the energy for each type of output between 0 and 100 % (e.g. 55% of green LO = 55% of 0.2 mJ 532 nm wavelength). There are three modes of laser modes: single, burst, and continuous. The laser pulse width is 4 ns and the system has a maximum frequency of 50 Hz for the continuous mode. The laser is focused using a 40x objective microscope (FS60, Mitutoyo, Japan). The Mitutoyo

microscope transmits 35% of the 532 nm wavelength energy and only 17% of the 355 nm wavelength energy [39]. Therefore, although gold is more absorbing at 355 nm than 532 nm, the transmission loss through the microscope makes 532 nm the better wavelength for ablation of gold.

A software-controlled XY shutter shapes the laser beam into a rectangle shape; minimum aperture of 2x2 µm to maximum aperture of 50x50 µm for 40x objective. A software mask can be designed in the laser system and a XY stage is used to translate the substrate according the laser patterns. The translation stage has a positioning precision of 1 µm and the scan rate can be set by the laser software. Schematic of the laser system is shown in Figure 6.

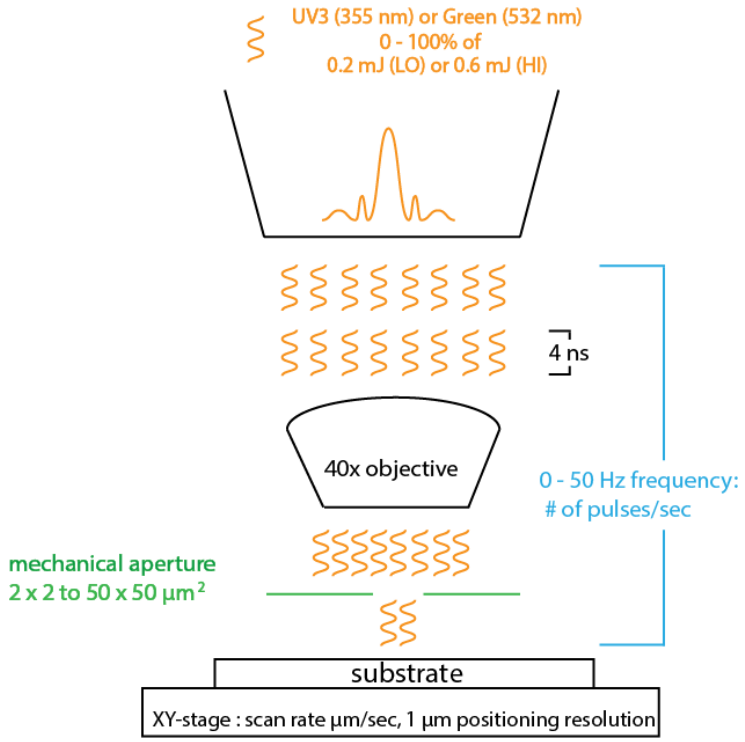

Figure 6. Schematic of the Quiklaze 50-ST2 system. A 4 ns pulsed 355 or 532 nm wavelength laser is generated by the system and focused using a 40x objective lense and passed through a mechanical aperture before ablating the surface of the substrate

For ablation of gold, green wavelength energy is used at a maximum aperture of 50x50 µm. Simple line patterns with different power output were used to determine the minimum threshold setting for ablation of gold. The output energy started at 10%, in increments of 5%, of a 0.2 mJ (LO) green laser with a frequency of 10 Hz in continuous mode. The 40x objective microscope mounted on the laser system is used for capturing images of the laser ablation of gold. The effect of ablation is visually noticeable as well as the lack of effect by the green wavelength laser on the PI.

2.1.2 Laser ablation of PI/Au and PI/Au/PI substrates

Laser ablation is dependent on the absorbance of the laser by the material of interest and the absorbance can change based on substrate layout. Two different substrates will be considered for ablation of PI: polyimide/gold/polyimide (section 2.1.2.1) and polyimide/gold substrate (section 2.1.2.2).

2.1.2.1 Laser ablation of PI/Au/PI substrate

Polyimide is spun on silicon substrate using methods described in section 2.1.1. An adhesion layer of 50 nm chrome and a 200 nm of gold are evaporated onto the polyimide. Lastly, another 10 µm polyimide layer is spun on and cured. Schematic of the substrate is shown in Figure 7.

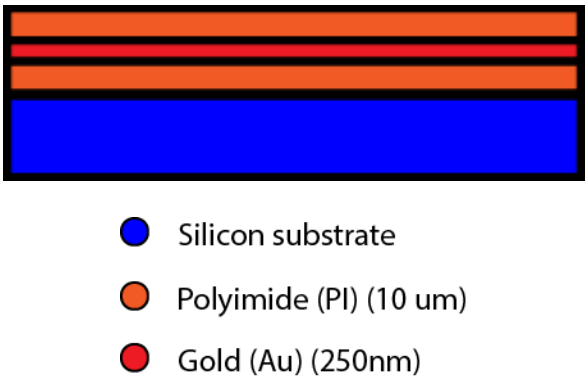

Figure 7. Schematic of polyimide/gold/polyimide substrate used for ablation of polyimide

First, a high power UV3 (HI) laser is used to remove bulk of the polyimide. Four 12.5 x 12.5 µm square UV3 (HI) mask lines of 80% intensity at 10 Hz with a scan rate of 35 µm/sec is used to ablate the 10 µm thick polyimide. After the mask lines are ablated, the substrate is imaged using the 40x objective microscope mounted on the laser system.

Once an observation is made, the laser power is reduced to UV3 (LO) laser with output energy of 35% (10 Hz, 12.5 12.5 x 12.5 µm square aperture). The substrate is imaged after each repetition of the mask lines until visible damage to the gold layer is observed to determine the threshold setting for removal of polyimide prior to gold layer damage.

To investigate the effect of laser beam size on ablation damage on gold during removal of polyimide, varying sizes of laser beam sizes at different power output was used to ablate gold on a gold/polyimide substrate after the top polyimide layer was completely ablated. UV3 (LO) laser was used with the power outputs of 20%, 30%, 40%, 50%, and 60% at aperture sizes of 2 x 2, 5 x 5, 10 x 10, 25 x 25, 50 x 50 µm. The scan rate of each ablation pass was 45 µm/sec and each

line was repeated 10 times or until visible damage on the gold was observed. The surface of the gold was imaged using the microscope mounted on the laser system.

2.1.2.2 Laser ablation of PI/Au substrate

A 50 nm chromium layer is evaporated as adhesion layer on clean silicon substrate followed by evaporation of a 200 nm thick gold layer. Next, a 10 µm polyimide is spun on and cured. A combination of 40 single shots of UV3 (HI) laser with output power of 30% and 20 shots of UV3 (HI) with 15% output power, both at 50 x 50 µm square aperture with 40 Hz frequency, is used to ablate the polyimide layer deposited on top of the gold layer without damaging the electrode layer. The resulting substrate is imaged using LEXT-OLS4000 laser confocal microscope. Schematic of the ablation process is shown in Figure 8.

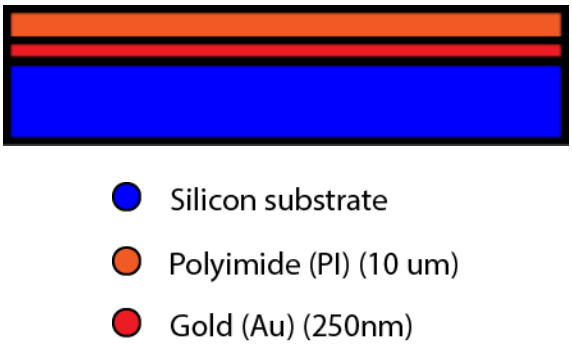

Figure 8. Schematic of gold/polyimide substrate used for ablation of polyimide

The LEXT-OLS4000 (Olympus, Central Valley, PA) laser confocal system has multiple objective lenses starting from 5x, 10x, 20x, 50x, and 100x magnifications. The LEXT-OLS4000 uses dual confocal optical system, which allows clear capture of substrates with different reflectance characteristics.

2.2 Impedance characteristics of polymer brush coated electrodes

A microelectrode array set was modified with polymer brush coating procedure [40]. Complex impedance measurements of the electrode were made before and after polymer brush coating. An Agilent 4294A impedance analyzer is used for obtaining impedance measurement. The analyzer is calibrated from 40 Hz to 1 MHz prior to each measurement and a frequency sweep using 100 mV signal is used to measure the impedance. Two-point measuring mode is used for measuring the impedance of the contact openings in phosphate buffer solution (PBS; monobasic potassium phosphate, sodium chloride, and dibasic sodium phosphate) (Gibco, Grand Island, NY), which emulate physiological conditions. One contact lead is connected to the gold layer and a flame-cleaned platinum wire is used as the counter electrode. The impedance at 1 KHz is used for comparison of pre- and post-polymer brush coating change in impedance at the electrode contact site. In most literature, the 1 kHz impedance is the point of focus since the frequency band from 300 Hz to 1 kHz is the band in which most neurons communicate with each other [41] and most experimental and clinical impedance measuring devices are set to measure the impedance value at 1 kHz [42].

2.3 Electrochemical deposition of platinum using macroporous polystyrene bead template

The electrochemical deposition of platinum using the PS template process starts with depositing either mono or multi-layers of PS beads in the laser-ablated contact opening and electrochemically depositing platinum on the contact opening site in a chloroplatinic solution. Once the platinum film is plated, the PS template is rinsed away in a toluene solution. Section 2.3.1 describes polystyrene bead template deposition methods in detail and section 2.3.2

describes the electroplating experimental procedures. Figure 9 shows the overall schematic of the process.

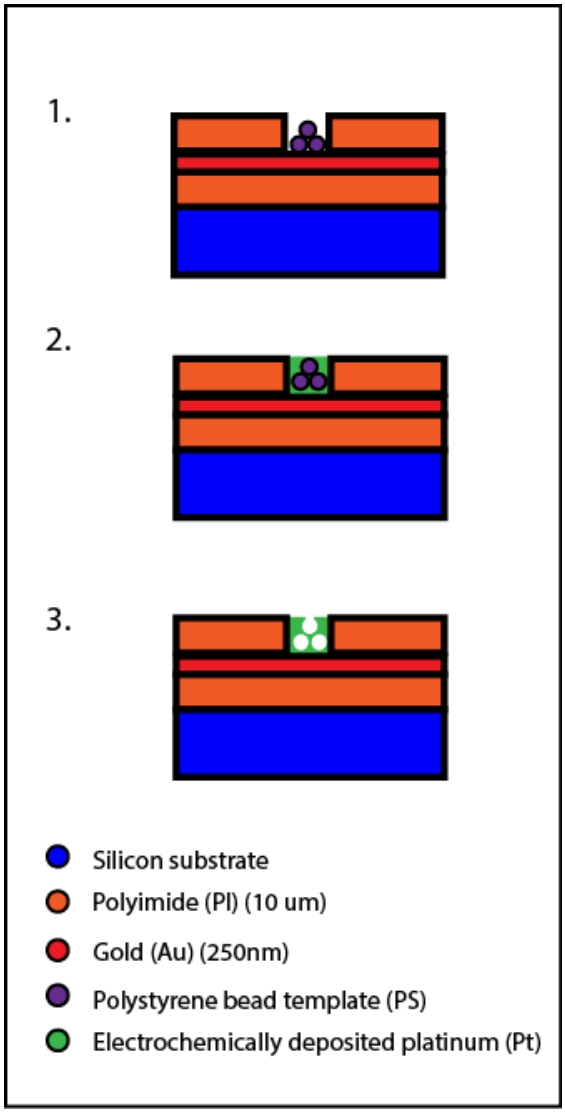

Figure 9. Process flow for electrochemical deposition of macroporous platinum film using latex polystyrene sphere template. 1) The PS beads are deposited using a pipette 2) Electrochemical deposition of macroporous platinum film 3) The PS bead template is dissolved in toluene solution

2.3.1 Cross-linked and non-cross-linked polystyrene beads for template formation

Two different volumes, 15 µL and 0.1 µL, are used for pipetting of 2 µm diameter, 2.6% wt PS beads. Initially, divinylbenzene (DVB) cross-linked PS beads (Bang labs, Fisher, Indiana) are used for template formation. Uncross-linked (Polysciences, Warrington, Pennsylvania) PS beads are also used for template formation as well. Before the PS beads are deposited, the substrate is sonicated in IPA for 30 minutes and rinsed with DI water. DVB cross-linked PS beads are more resilient to solvents and possibly non-optimal for formation of PS templates. The beads are cleaned using centrifugation to replace the water in the solution with DI water. This process is repeated three times. The beads are deposited on the contact opening area using a pipette and dried overnight unperturbed in room temperature setting. To test removal of PS, the templated substrate is submerged in toluene solution, initially heated to 110°C for 30 minutes, then cooled to room temperature and left in solution for 24 hours. The substrate is then rinsed with acetone, IPA, and DI water and gently dried with air stream.

2.3.1.1 Drying in saturated humidity chamber (99%) vs. ambient room environment

The PS solution is evaporated in two different humidity settings, 99% humidity and ambient room humidity, to observe if humidity settings modulate uniformity of the PS template within the contact openings. Five samples for each humidity environments were templated with PS solution and left to evaporate over a period of 24 hours. An Espec LHU-113 (Hudsonville, MI) humidity chamber is used to create a 99% humidity setting for evaporation of PS solution. After the PS template is formed, the substrates are imaged using the LEXT-OLS4000 confocal laser microscope for visual comparisons.

2.3.1.2 Inkjet printing of PS beads

To further control the amount of PS solution deposited for template formation, inkjet printer is used to deposit Pico-liter range of PS solution. Drop-on-demand piezoelectric inkjet printing was used to deposit 2 µm diameter, polystyrene bead suspension on a laser-ablated contact opening. An inkjet nozzle with an orifice of 80 µm (MicroFAB MJ-ABP-01) was utilized for this experiment. It was actuated with an arbitrary function generator (Agilent 33220A) in series with a 50x amplifier (TRek Model 603) to produce a ±22.5 V peak-to-peak, 60 Hz bipolar waveform. Once the inkjet was aligned with the target on the substrate, droplet ejection from the inkjet nozzle was triggered by a button press on the user interface of the arbitrary function generator. This causes the piezoelectric element embedded within the center of the inkjet channel to contract producing a single droplet to be ejected with a volume of 115 pL. The bead suspension was supplied to the inkjet by gravitation forces.

2.3.2 Electrochemical deposition of platinum

The experimental setup for electrochemical deposition is the same for all three types of deposition, as shown in Figure 10. The voltage/current at the working electrode is varied for the three types of electroplating: galvanostatic or constant current mode deposition (section 2.3.2.1,) potentiostatic or constant voltage mode deposition (section 2.3.2.2,) and pulsed-potentiostatic or pulsed-voltage mode (section 2.3.2.3). Chloroplatinic acid hydrate was obtained from Sigma Aldrich (purity 99.9995%) and a 0.095 M solution was prepared for all electrochemical deposition process. A µAUTOLABIII (Utrecht, Netherlands) system is used for all the electrochemistry process. The working electrode is attached to the gold metal layer through an electrode contact and a 10 mL of the 0.095 M chloroplatinic acid solution is pipetted onto the

contact opening. A platinum (Pt) wire is used as the counter electrode, which the reference electrode was connected to. The Pt wire is flamed prior deposition to remove any impurities. The electrochemistry process is then carried out using the three different modes. After electroplating, the PS beads are dissolved in toluene as previously described and the macroporous platinum film is imaged using the LEXT-OLS4000 microscope.

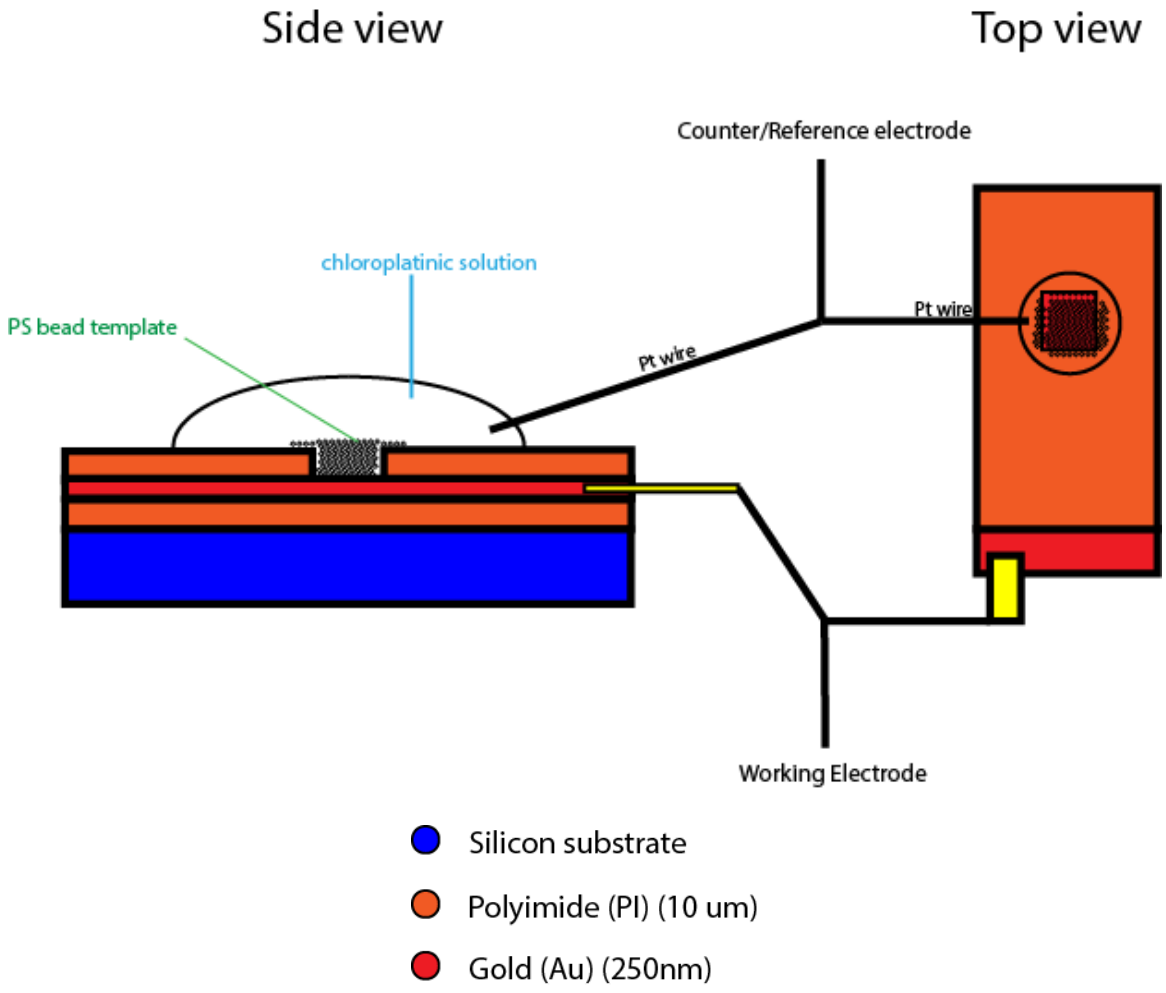

Figure 10. Experimental setup for electrochemical deposition of platinum. Top view shows the localized droplet size of the chloroplatinic solution used for electroplating and the location of the working electrode contact pad. Side view shows the substrate layout and a schematic of how the counter/reference electrode Pt wire was dipped into the chloroplatinic solution

2.3.2.1 Galvanostatic mode deposition

Five samples of 50x50 µm contact openings templated with 2 µm diameter uncross-linked PS beads are used for galvanostatic mode deposition. The current was set at 6 µA and the deposition time was 150 seconds. After deposition, the PS beads are rinsed in toluene solution overnight. The substrates are submerged in toluene solution that is initially heated up to 110 °C for 30 minutes, then cooled to room temperature and left in solution for 24 hours. The substrate is then sequentially rinsed in acetone, IPA, and DI water and gently dried with air gun. The resulting platinum film is observed using the LEXT-4000 confocal laser microscope at an objective of 100x.

2.3.2.2 Potentiostatic mode deposition

Five samples of 50x50 µm contact openings templated with 2 µm diameter uncross-linked PS beads are used for potentiostatic mode deposition. The voltage was set at -1.0 V at the working electrode and the deposition time was 150 seconds. After deposition, the PS beads are removed in toluene solution as described previously. The resulting platinum film is observed using the LEXT-4000 confocal laser microscope at an objective of 100x.

2.3.2.3 Pulsed-potentiostatic mode deposition

Five samples of 50x50 µm contact openings templated with 2 µm diameter uncross-linked PS beads are used for pulsed-potentiostatic mode deposition. The working electrode is set at -0.9 V voltage with 5 second “ON” and 10 second “OFF” modulation, for 80 pulses. After deposition, the PS beads are rinsed in toluene solution overnight. The substrates are submerged in toluene solution is initially heated up to 110°C for 30 minutes, then cooled to room temperature and left

in solution for 24 hours. The substrate is then rinsed in acetone, IPA, and DI water respectively and gently dried with air gun. The resulting platinum film is observed using the LEXT-4000 confocal laser microscope at an objective of 100x.

2.3.3 Impedance characteristics of electroplated electrodes and surface area analysis

The setup for measuring impedance is similar to the electrochemistry setup; 10 mL of phosphate buffer solution (monobasic potassium phosphate, sodium chloride, and dibasic sodium phosphate) obtained from Gibco is pipetted onto the substrate and one of the measurement leads for the Agilent 4294A impedance analyzer is attached to the gold contact pad and the other lead is connected to the buffer solution through a flame-cleaned Pt wire. The phosphate buffer solution is used due to its similarity to physiological solution. The impedance value at 1 kHz is used for comparison of pre and post electroplating measurements. Complex impedance measurement of the pre- and post-modified electrode can be used to measure the change in surface area of the electrode based on the model discussed in Section 1.5.

2.3.4 Surface area measurement of macroporous platinum film

Typically, the total electro-chemically active surface area of platinum film is calculated using hydrogen underpotential deposition due to its characteristic monolayer formation. For platinum CV experiments, the platinum to-be-analyzed is first cleaned using previously mentioned methods of flaming to rid of impurities present on the surface of highly-active platinum films. However, cleaning methods for platinum film in this experiment are chemically and physically difficult without damaging the underlying thin film or the insulating polyimide.

Image analysis can be used to approximate the macro-surface area of the platinum film by incorporating calculations based on basic geometry of the polystyrene spheres with results from image analysis of the films. In implantable device, the nano-sized features on the platinum film would be masked due to polymer brush coating modifications which effectively passivate the platinum features.

Figure 11 shows an example surface area approximation of a macroporous film using image analysis—the red area is the flat platinum area where platinum is deposited in between the polystyrene spheres and the light blue area is surface area increase due to the spherical features of the polystyrene template. Depending on the thickness of the platinum deposition, the measured diameter of the spherical area from the top refers to a plane either above or below the plane passing through the center of the sphere. The exact plane can be determined from the result of current measurement during electroplating process as well post-electrodeposition thickness measurements. The LEXT OLS-4000 software has a profile measuring feature for measuring the electroplated platinum. After all of the impedance and image characterization, a thickness-reference gold layer opening will be ablated and the thickness of the platinum can be measured with respect to the new exposed gold layer for characterization of the electroplated platinum.

The surface area of the spherical cap is given by the following equation:

$$\boldsymbol{S_{cap} = \pi(a^2 + h^2)} \quad (5)$$

Where a is the measured diameter of the spherical cap from the top and h is the height of the spherical cap. The improvement in surface area can be approximated by adding the red flat area

with sum of all the spherical cap surface area and comparing the value to a flat unmodified geometrical surface area.

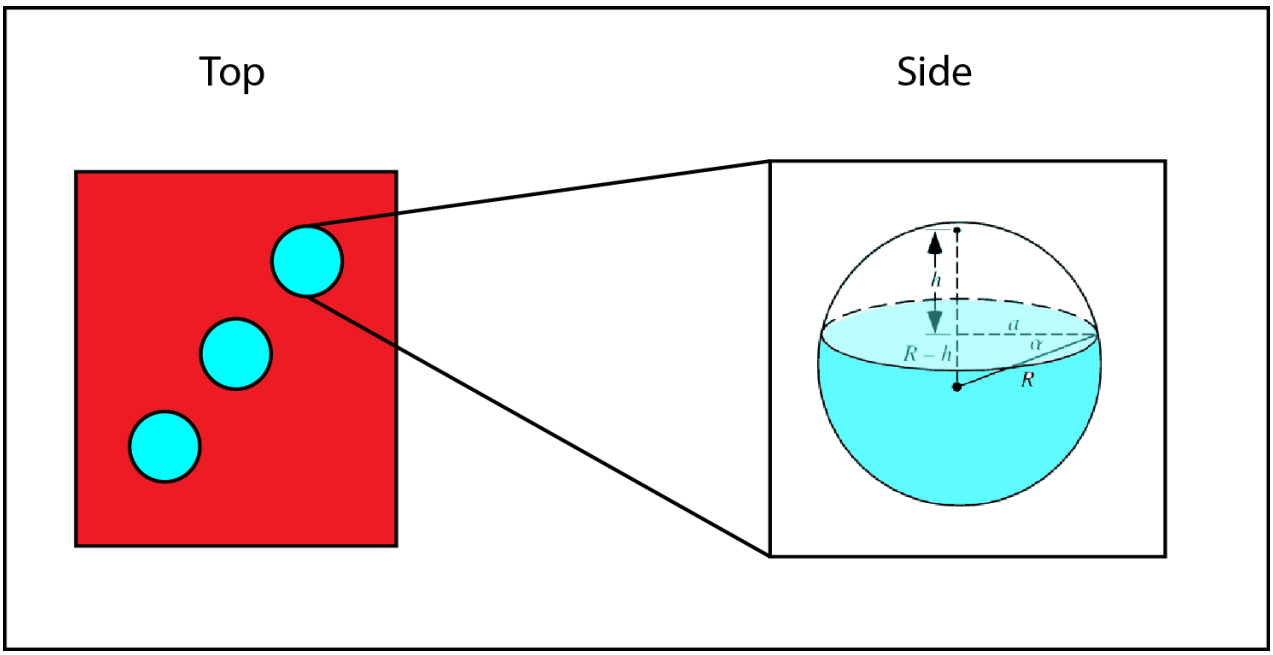

Figure 11. Image analysis of surface area of macroporous platinum film. Top view shows an example macroporous platinum film. The red area refers to flat platinum surface while the light blue indicates a platinum film that was deposited conformal to a PS bead. Side view of the spherical cap show the geometrical variables required for surface area calculation of the spherical cap

2.3.5 Polystyrene packing density in hexagon area

To investigate whether polystyrene beads pack more densely or uniformly in a different geometrical bound shape, a hexagon shaped contact opening was laser ablated and templated with 2 µm diameter uncross-linked PS beads. Platinum film was deposited using pulsed-potentiostatic electrochemical deposition with 80 pulses of -0.9 V potential with 33% duty cycle, 15 second period. The hexagon bound area has six equal sides of 35 µm and a total are of 3183 μm^2.

In another experiment to investigate PS bead packing, 0.7 μm diameter uncross-linked PS beads were used to template 50 x 50 μm square contact opening and platinum was deposited using 80 pulses of -0.9 V potential with 33% duty cycle, 15 second period.

After deposition of platinum in both experiments, the PS is rinsed away in toluene solution and the templated platinum films are imaged using the LEXT-OLS4000 microscope. Image analysis was used to determine the number of PS beads per bounded area to determine the PS packing density.

Chapter 3: Results

3.1 Laser ablation

3.1.1 Laser ablation of gold

The threshold power required for ablation of a 200 nm thick gold film starts at 15% of green (LO) laser, as shown in Figure 12. The two different laser energy used to ablate the two tracks shown were 15% and 20% output of a 0.2 mJ (LO) green Nd:YAG laser, shot at a frequency of 10 Hz at a scan rate of 30 µm/sec. The 15% laser leaves visible laser gold particle strands whereas the 20% laser completely ablates the gold layer. No visible ablation of the polyimide layer underneath is observed.

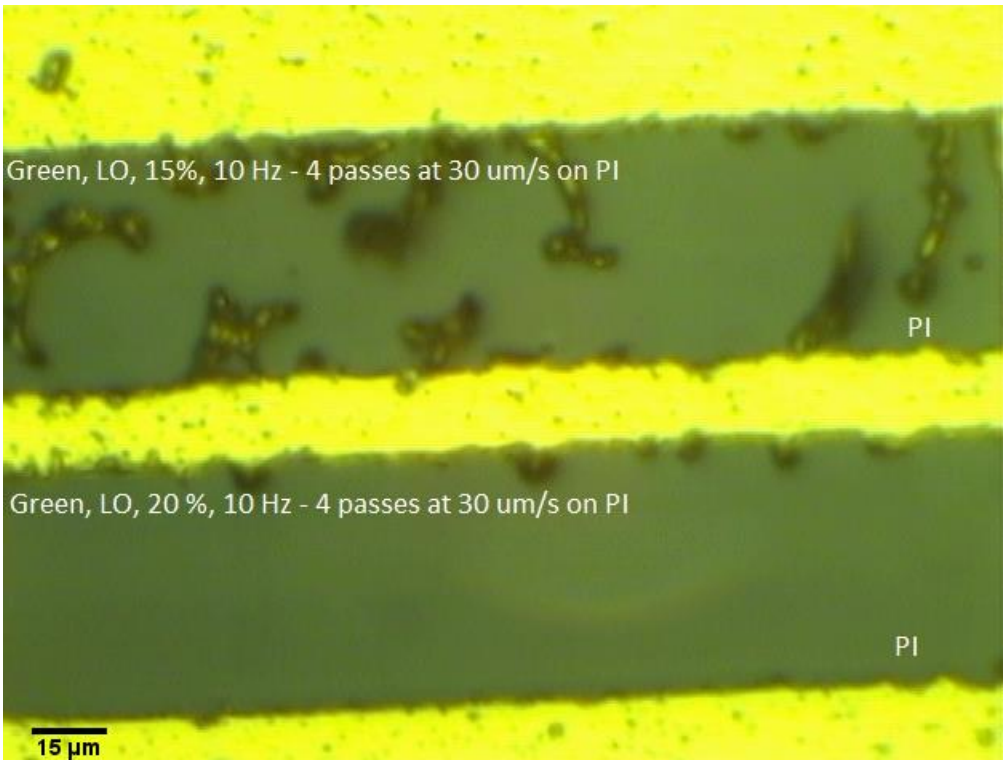

Figure 12. Laser ablation of gold on a gold/polyimide/glass substrate. The ablation path on top show visible gold particle residue. In the bottom path, the gold layer is completely ablated

To observe the effect of laser ablation of the polyimide layer, a 355 nm (UV3) Nd:YAG laser is used to ablate the exposed polyimide on the same substrate. The laser setting used is 15 and 20 % of 0.6 mJ (HI) UV3 laser at a 30 µm/sec scan rate. When the PI is ablated by the lower energy (15%) laser, ablation marks from the laser is observed on the PI surface, as seen in top part of Figure 13. The 20% output laser completely ablates the PI and exposes the glass substrate underneath. Partial PI is observed on the sides due to the laser turning on/off at the start/end of the laser path, respectively, thus decreasing the number of repetitions of laser ablation on the outside edges of the path.

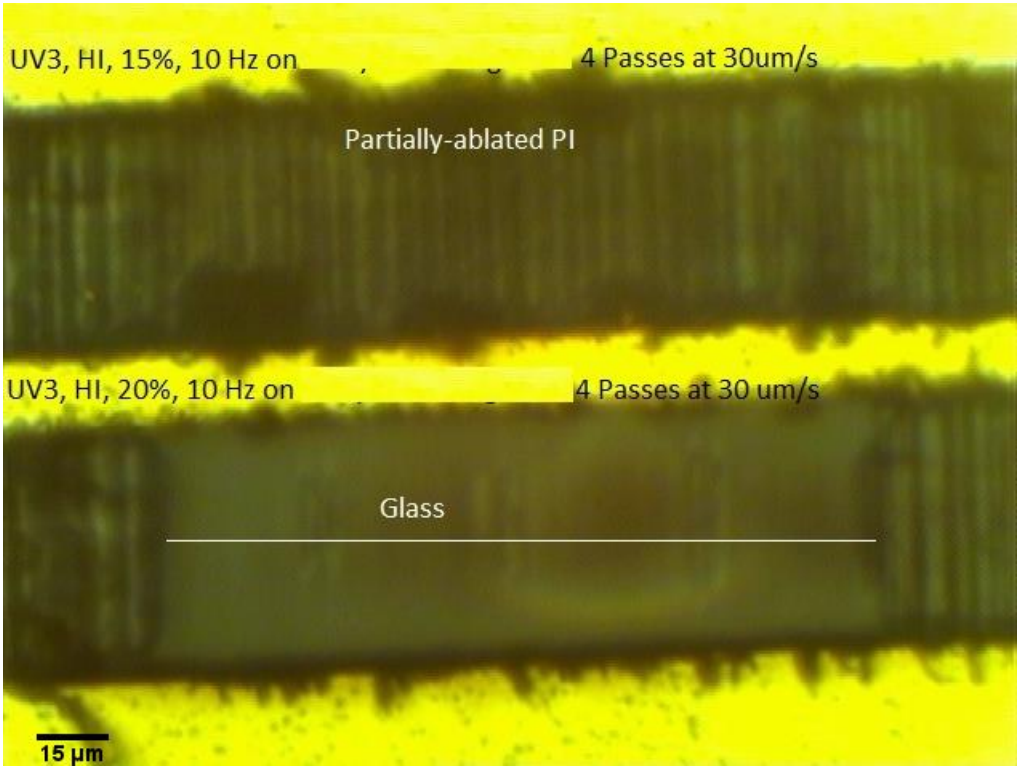

Figure 13. Laser ablation of the exposed polyimide layer from Fig. 8. In the top path, the laser power was not powerful enough to completely remove the polyimide whereas all the polyimide is removed in the bottom path. The vertical lines observed in the partially ablated polyimide are due to the scan rate of the laser path. Polyimide is still present on the edges of the bottom path due to the delay in the laser turning on when starting or finishing a laser path

3.1.2 Laser ablation of PI while stopping on top of gold

The parameters for laser ablation of PI on top of gold depend on the overall substrate material layout. The effect of laser on the PI/Au layer is different than that of a PI/Au/PI layer due to different absorbance characteristics of each layout configuration. Section 3.1.2.1 shows the result of ablation of polyimide on PI/Au/PI substrate whereas section 3.1.2.2 shows the result of ablation of polyimide on PI/Au substrate.

3.1.2.1 Laser ablation of PI/Au/PI substrate

A UV3 (HI) laser with output energy of 80% (10 Hz, 12.5 x 12.5 µm square aperture) is used to ablate PI on top of a gold/polyimide surface at 35 µm/sec rate, as seen in Figure 14. Most of the PI is ablated while no visible damage to the gold is observed.

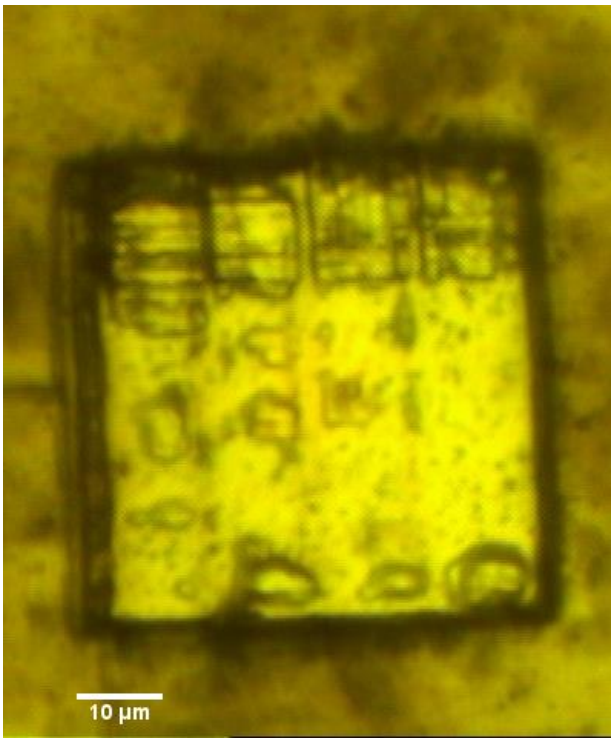

Figure 14. Laser ablation of polyimide using UV3 HI laser (10 Hz, 80%, 1 pass at 35 um/sec, 12.5 x 12.5 µm aperture)

Next, a UV3 (LO) laser with output energy of 35% (10 Hz, 12.5 12.5 x 12.5 µm square aperture) is used to ablate the same path 3 times at 35 µm/sec rate, as seen in Figure 15. More of the PI is removed while the gold layer is still intact.

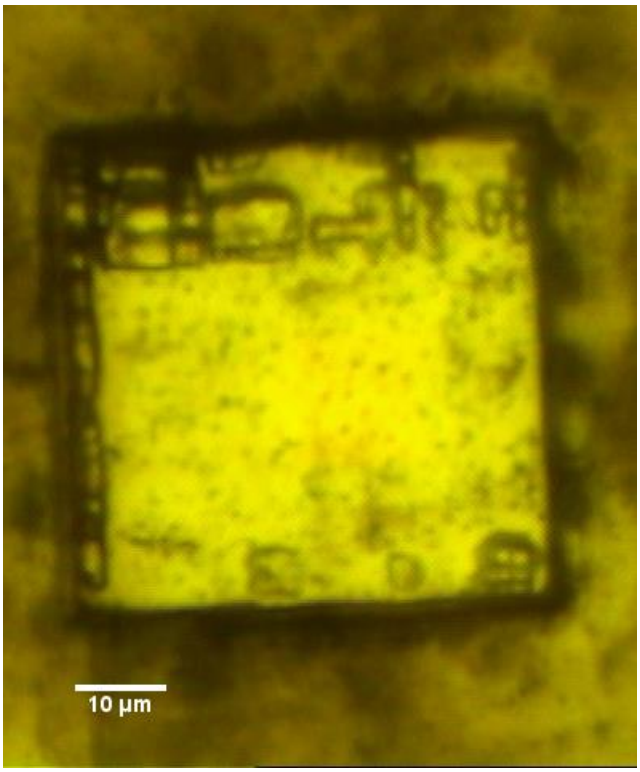

Figure 15. Laser ablation of polyimide using UV3 LO laser (10 Hz, 35%, 3 passes at 35 um/sec , 12.5 x 12.5 µm aperture)

However, one more additional pass of the 35% UV3 (LO) at the same parameter starts to ablate the gold layer and a visible "crack" is observed, as seen in Figure 16.

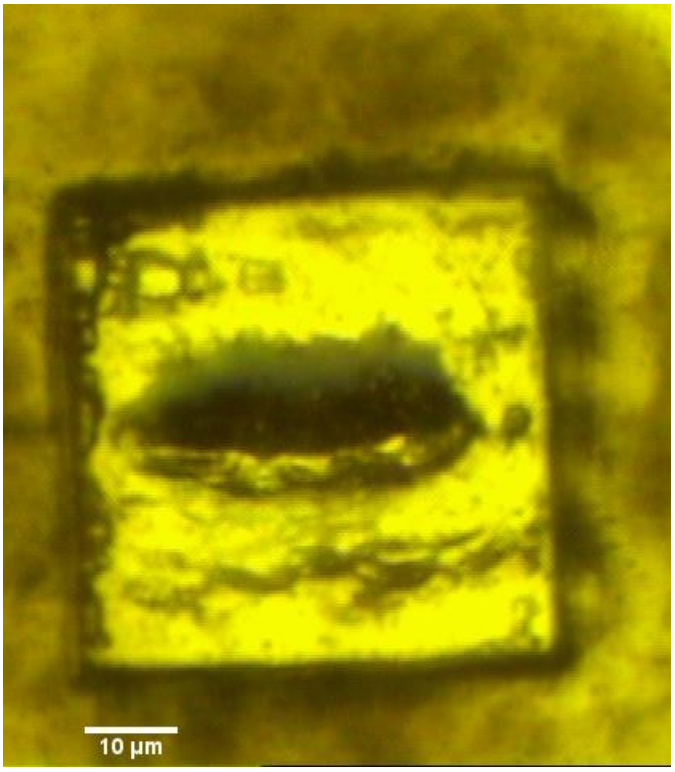

Figure 16. The gold substrate shown in Fig. 11 is damaged after one more additional pass of UV3 LO laser (10 Hz, 35%, 1 pass at 35 um/sec, 12.5 x 12.5 um)

The ablation of gold by UV3 laser is noticeably different than that of ablation by green laser. The UV3 laser seems to melt (thermal-ablation) the gold whereas green laser photoablates the gold. The polyimide layer was completely removed without damaging the gold substrate with the following parameters: 1 pass of UV3 HI laser (10 Hz, 80%), 3 passes of UV3 LO laser (10 Hz, 35%) and 3 passes of UV3 LO (15% output, 10 Hz) all at a scan rate of 35 µm/sec with 12.5 x 12.5 µm aperture), as shown in Figure 17.

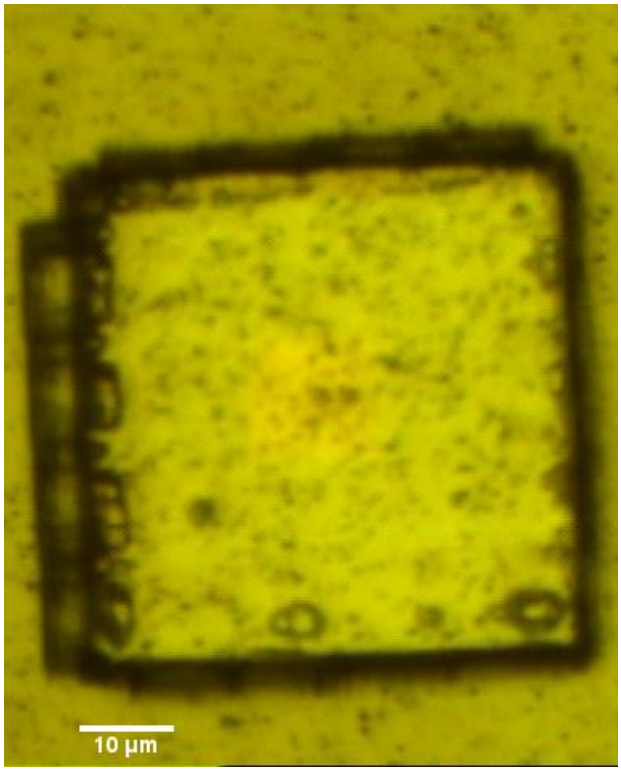

Figure 17. Complete removal polyimide after using combination of UV lasers: 1 pass of UV3 HI laser (10 Hz, 80%), 3 passes of UV3 LO laser (10 Hz, 35%) and 3 passes of UV3 LO (15% output, 10 Hz) all at a scan rate of 35 µm/sec with 12.5 x 12.5 µm aperture)

To test for complete removal of PI by laser ablation, two 600 x 600 µm contact pads were laser ablated on different sides of a rectangular substrate and tested for electrical conductivity using a digital multi meter. Electrical connectivity was observed only between the two pads on the whole substrate. The schematic of the test structure is seen in Figure 18.

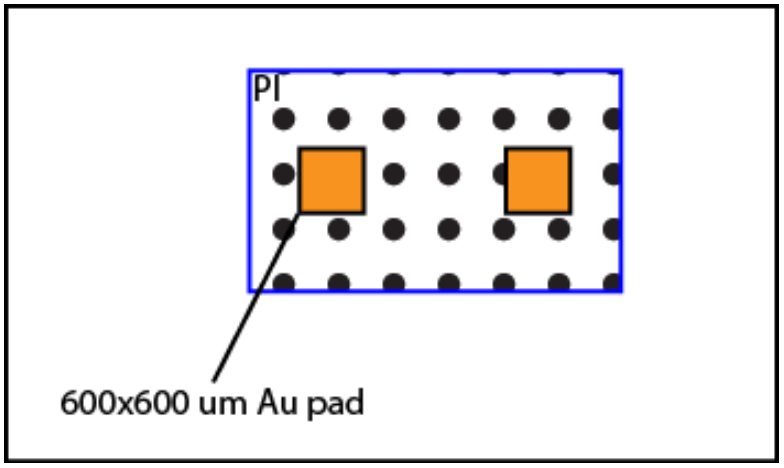

Figure 18. Schematic of a test structure used to investigate complete removal of polyimide using laser ablation

The results of varying laser beam size ablations are summarized in Table 1. The gold surfaces were visually inspected after each ablation pass for damage on the gold surface. A maximum of 10 passes was run unless the gold layer was damaged during ablation. Larger laser beam sizes at higher output power resulted in more severe ablation damage on the gold surface. Figure 19 shows damage on the gold and polyimide surface as a result of 60% output of UV3 LO laser at an aperture of 50 x 50 µm while Figure 20 shows ablation damage from the same size laser beam at 40% power output. Figure 21 shows ablation damage from a UV3 LO laser at 60% output with a beam size of 25 x 25 µm. The output power on the 2 x 2 µm beam size was increased until damage could be observed on the gold surface as well. When the output power was at 80% of UV3 LO, ablation damage could be observed on the gold surface from the 2 x 2 µm beam size.

Table 1. Number values indicate the number of passes before visible damage on the gold surface was observed and a check indicates no visible damage on the gold surface after 10 passes. The UV3 LO laser had output powers of 20, 30, 40, 50, and 60 %, all with a scan rate of 45 µm/s

	20%	30%	40%	50%	60%
2 x 2 µm	✓	✓	✓	✓	✓
5 x 5 µm	✓	✓	✓	✓	✓
10 x 10 µm	✓	✓	✓	3	2
25 x 25 µm	✓	✓	2	1	1
50 x 50 µm	✓	2	1	1	1

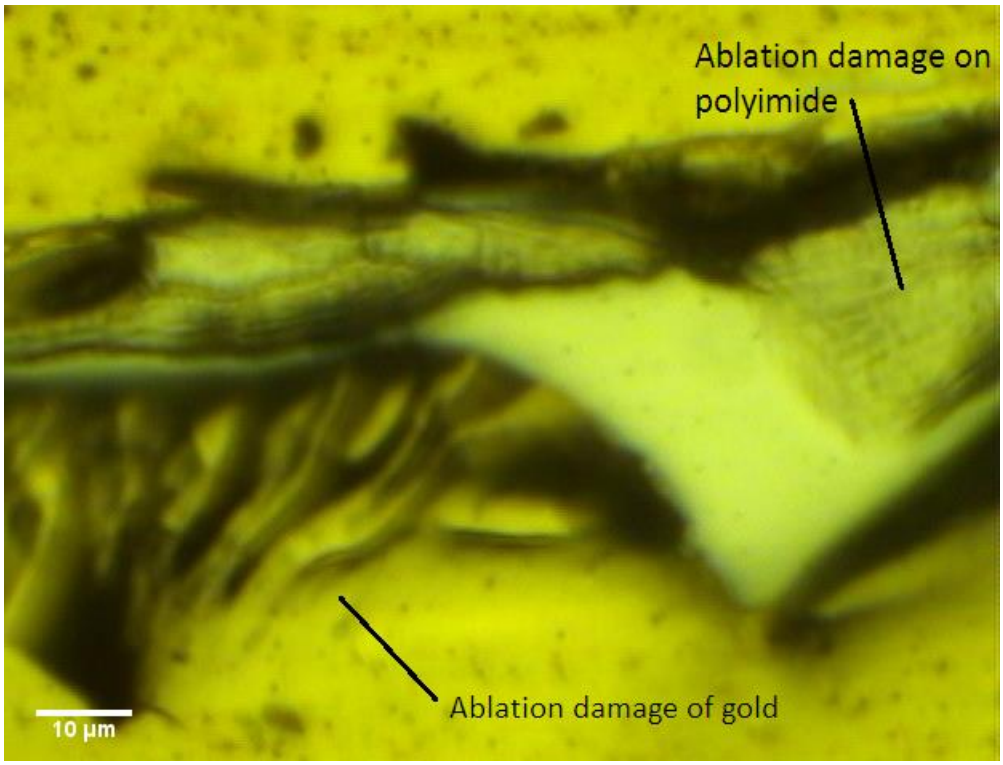

Figure 19. Ablation damage on the gold surface as a result of 60% output of UV3 LO at 50 x 50 µm. The polyimide layer underneath is also damaged from the ablation as well

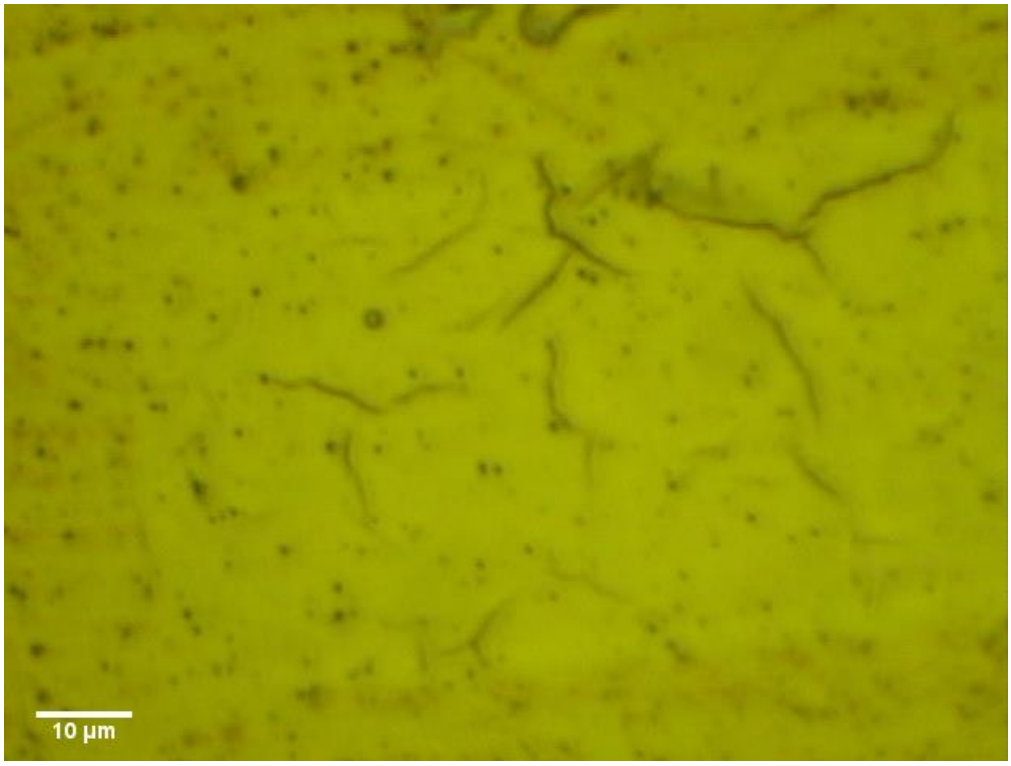

Figure 20. Ablation damage on the gold surface as a result of 40% output of UV3 LO at 50 x 50 µm.

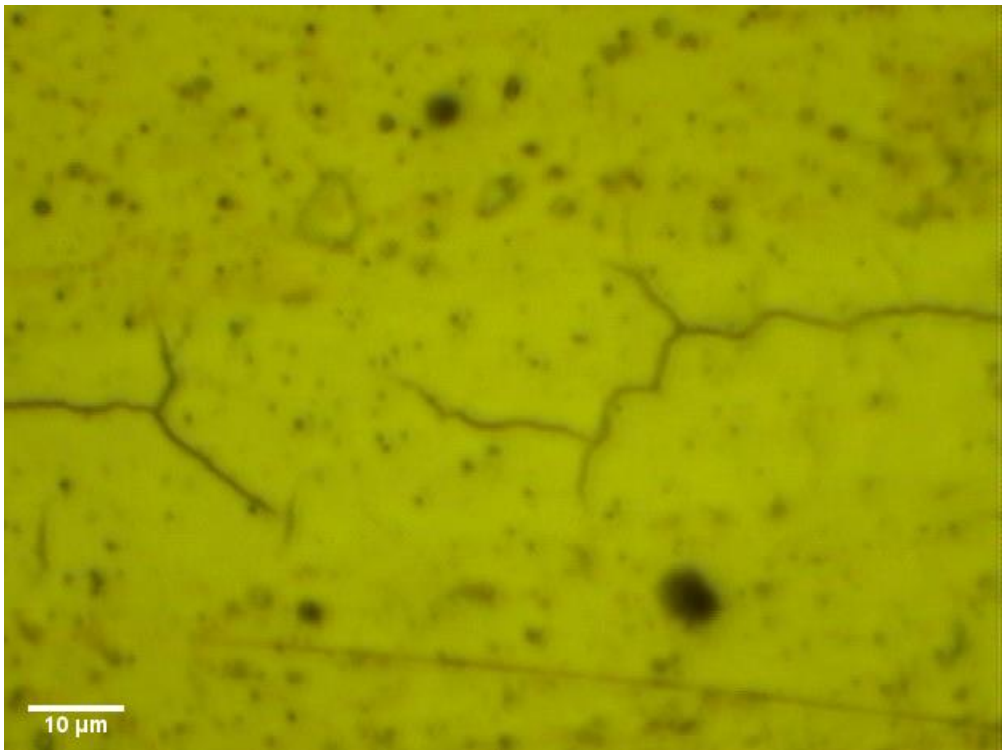

Figure 21. Ablation damage on the gold surface as a result of 60% output of UV3 LO at 25 x 25 µm

3.1.2.2 Laser ablation of PI/Au substrate

The polyimide was completely ablated while no ablation damage was observed on the gold surface when using combination of 40 single shots of UV3 (HI) laser with output power of 30% and 20 shots of UV3 (HI) with 15% output power, both at 50 x 50 µm square apertures with 40 Hz frequency. The result is shown in Figure 22.

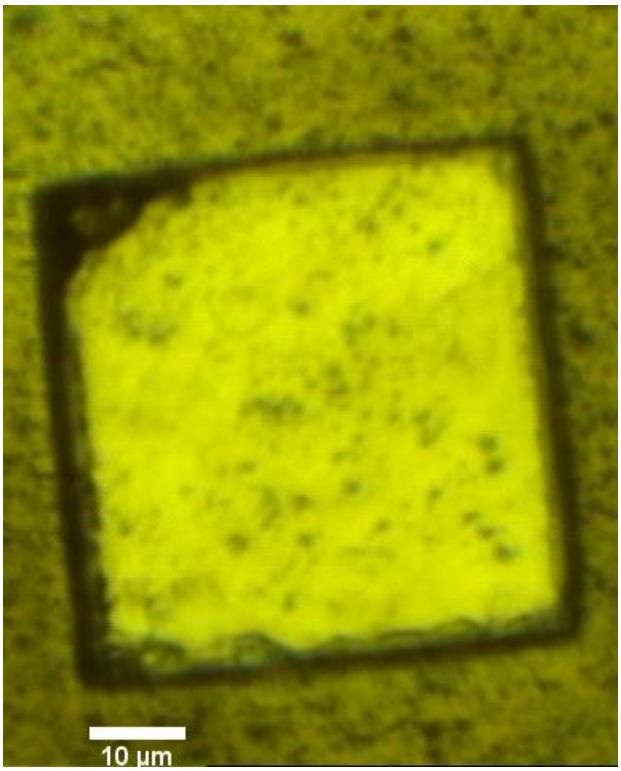

Figure 22. Complete ablation of polyimide using 40 single shots of UV3 (HI) laser with output power of 30% and 20 shots of UV3 (HI) with 15% output power, both at 50 x 50 µm square apertures with 40 Hz frequency on a polyimide/gold substrate

3.2 Impedance characteristics of polymer brush coated electrodes

After the polymer brush coating, an increase in impedance was observed in all the modified electrodes. The pre-modification 1 kHz impedance value is 1.45 ± 0.313 MΩ (N=5) and post-

modification 1 kHz impedance value is 3.642 ± 0.718 MΩ (N=5). On average, the polymer brush coating increased the impedance of the electrode contact opening by a factor of 2.55. Figure 23 shows the complex impedance measurement of a post-modified electrode.

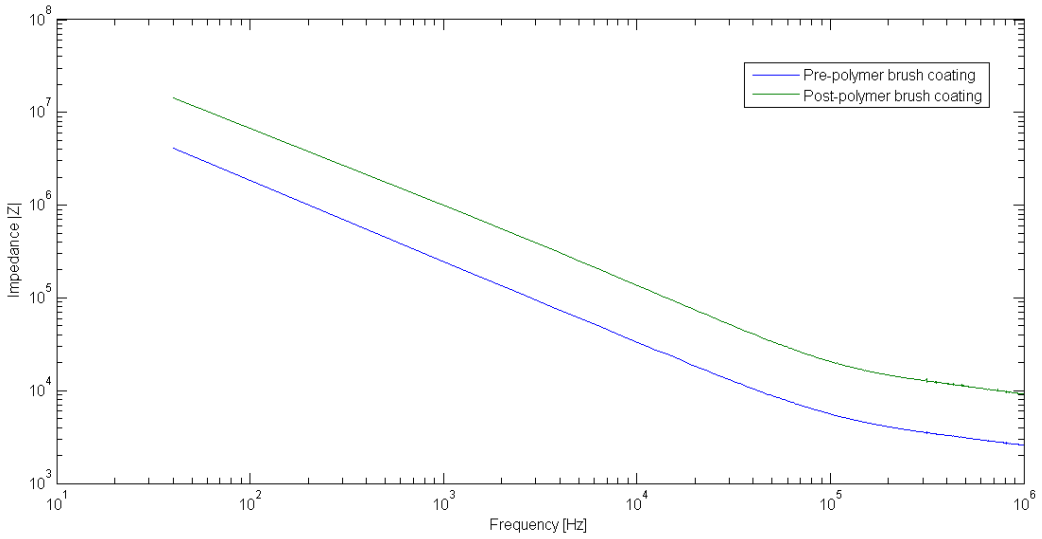

Figure 23. Complex impedance measurement of post-modified electrode, frequency range is from 40 Hz to 1 MHz

3.3 Electrochemical deposition of platinum using macroporous polystyrene bead template

3.3.1 Cross-linked and non-cross-linked polystyrene beads for template formation

There was no significant difference in filling of the electrode contact openings with PS beads based on different volumes of beads pipetted on the contact opening. Excess polystyrene beads were observed around the contact opening when 15 µL of polystyrene bead suspension was used. The excess PS had to be wiped during the electrochemical deposition to ensure enough platinum solution was present during electroplating as well. Images from pre and post-wiping indicated that the PS structure within the contact opening remained intact. Figure 24 shows a contact

opening filled using a 0.1 µL PS solution. The 10 µm thick contact opening is completely filled with PS.

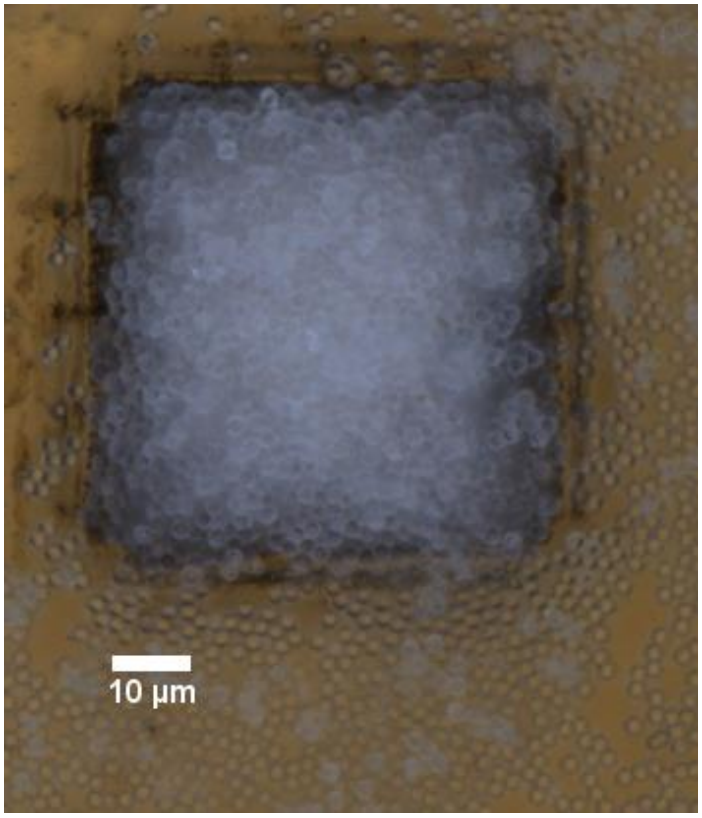

Figure 24. Contact opening (50x50 µm) filled with 2 µm diameter PS beads

The DVB cross-linked PS leaves a visible residue after toluene rinse. The residue is undesirable because the platinum site becomes contaminated and therefore a poor site for polymer brushes coating and other electrode modifications. No residue was observed after uncross-linked PS beads were rinsed in toluene. SEM imaging of the PS residue is seen in Figure 25 and Figure 26.

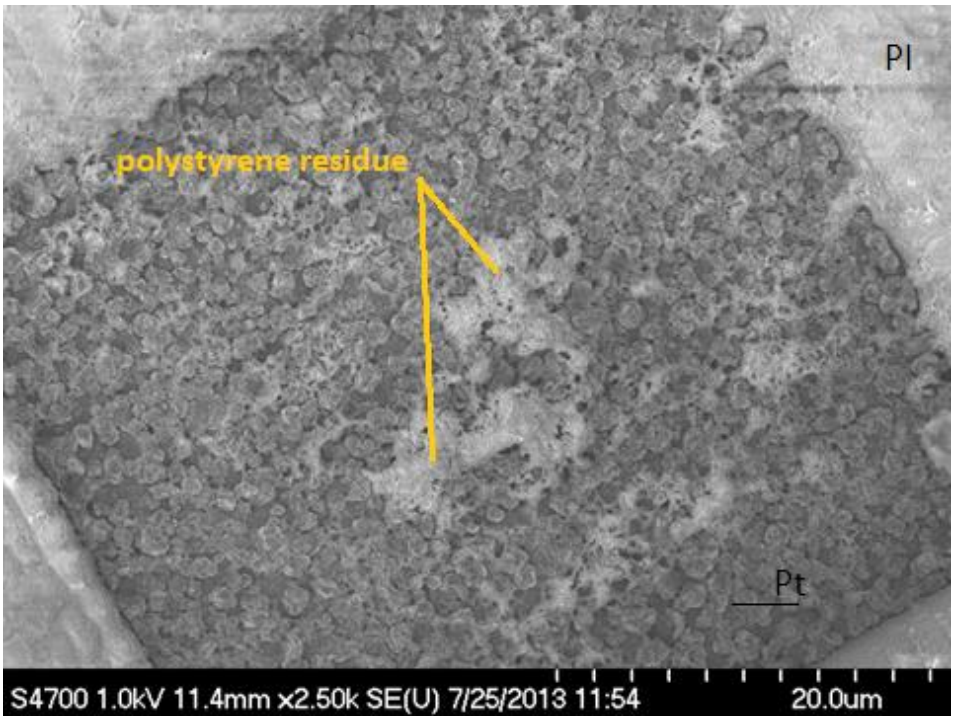

Figure 25. SEM image of a Pt electroplated contact opening after toluene rinse. Polystyrene residue is still visible on the surface

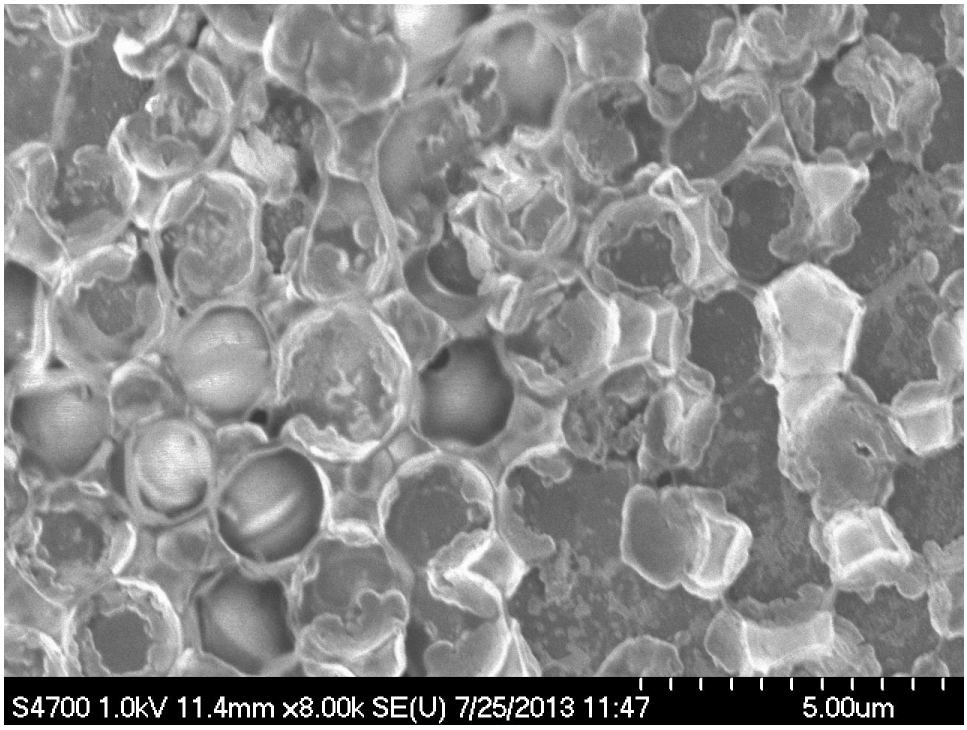

Figure 26. SEM image of polystyrene residue after toluene rinse

3.3.1.1 Saturated humidity chamber environment vs. ambient room environment

There is no visible difference in filling of contact openings with PS bead solution when the samples were dried in saturated humidity chamber or ambient room setting for the volumes of PS solution used (15 and 0.1 µL).

3.3.1.2 Inkjet printing of PS solution

Figure 27 demonstrates the difficulty of focusing inkjet droplets on the contact openings. The contact opening is outlined by a red square in the image. Three droplets from the inkjet printer, outlined in pink circles 1-3, were deposited near the contact opening, although none of them was directly applied onto the spot. Figure 28 shows the same contact opening at an objective of 100x zoom, in which it is clear that the gold layer is not completely filled with polystyrene beads.

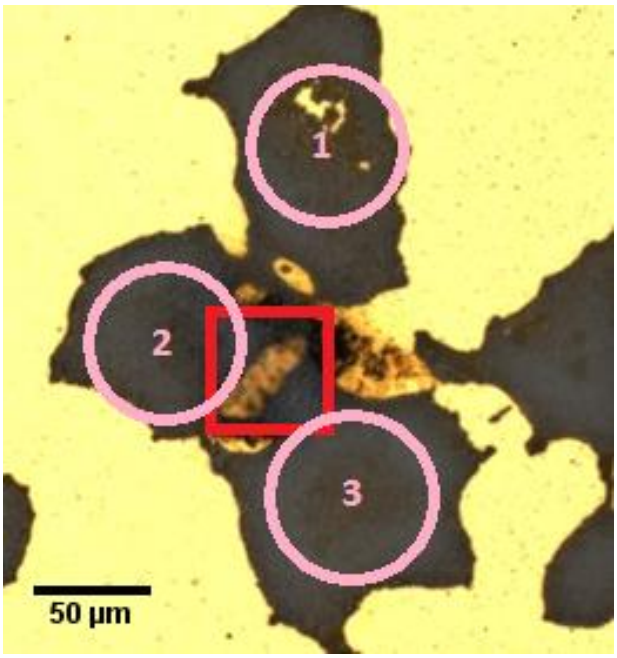

Figure 27. The contact opening, outlined in the red square, is partially filled with polystyrene beads from 3 different inkjet droplets, outlined in 3 pink circles, near the contact opening

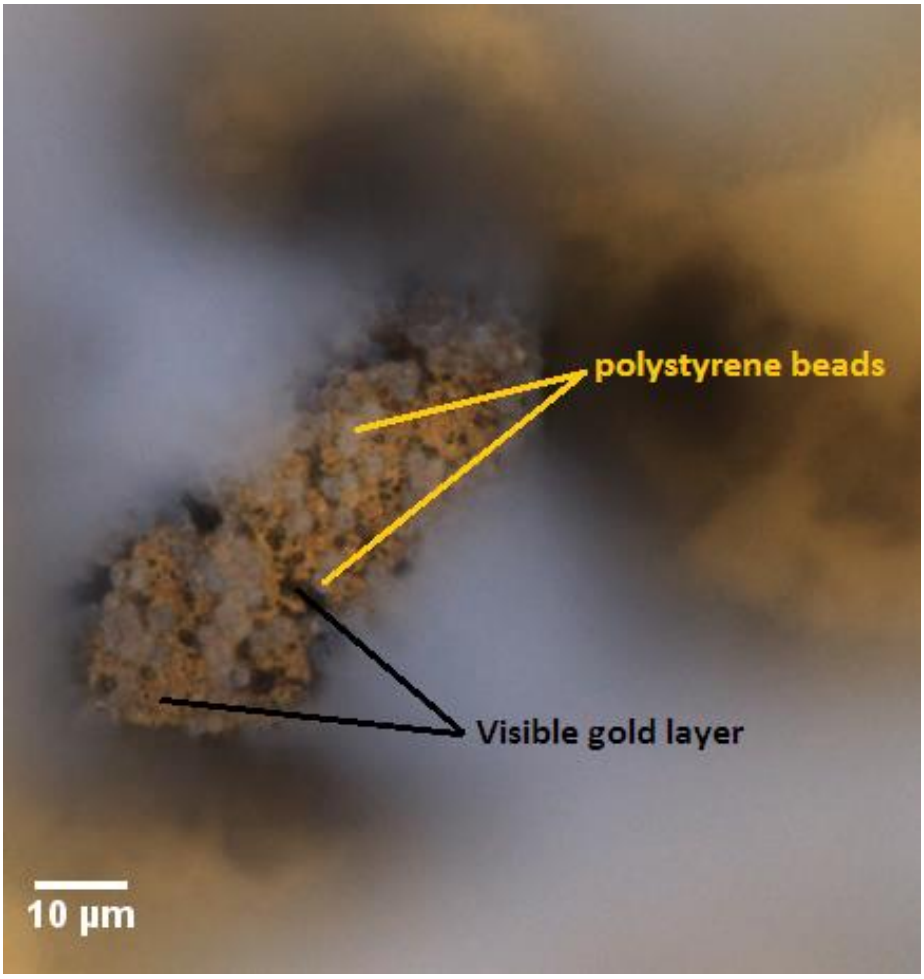

Figure 28. Zoomed in (100x) image of the red square outline from Figure 22. The transparent objects seen are the 2 µm polystyrene beads, which does not completely fill the contact opening. The microscope is focused on the surface of the gold, therefore the thick layers of polystrene beads is out-of-focus in the image

Figure 29 shows another contact opening, outlined by a light blue box, with better deposition of polystyrene beads from an inkjet printing droplet. The contact opening is filled with polystyrene beads from three separate inkjet droplet, therefore it is possible that the template structure is non-uniform. The middle of the contact opening is observed to be more translucent, which indicate either a thin layer of polystyrene in the middle or a bead-free area on the gold surface.

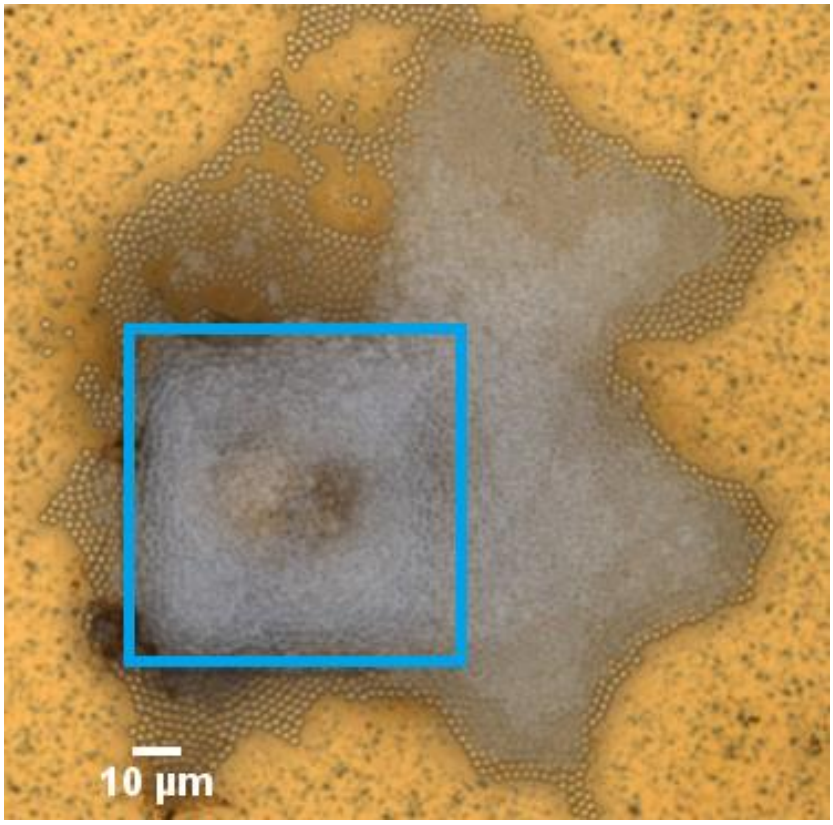

Figure 29. A contact opening completely filled with inkjet printed PS solution

3.3.2 Electrochemical deposition of platinum

Three different electroplating process results are discussed in the following section: galvanostatic mode (section 3.3.2.1) potentiostatic mode (section 3.3.2.2) and pulsed-potentiostatic mode (section 3.3.2.3).

3.3.2.1 Galvanostatic mode electrochemical deposition

A successful galvanostatic mode deposited platinum film is shown in the Figure 30. The surface of the platinum film is uneven since the gold layer is still visible in several regions within the contact opening. The platinum did conform to the polystyrene template, depositing in a shape of a spherical cap around the beads.

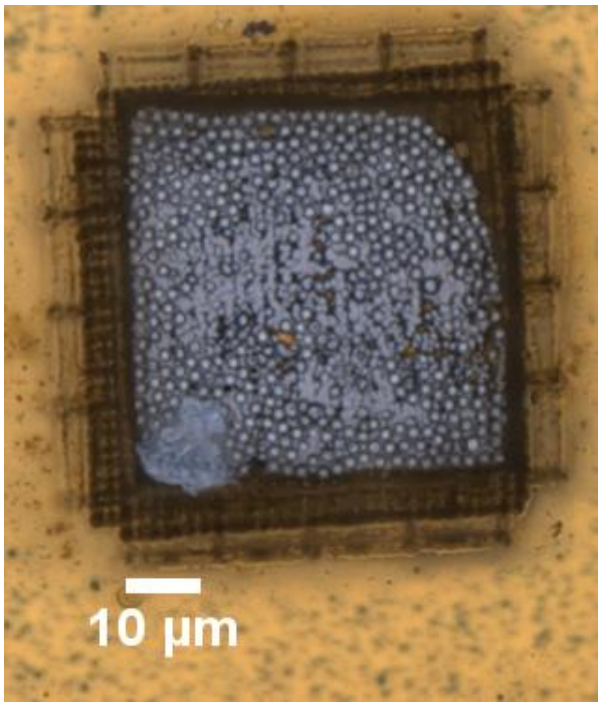

Figure 30. Galvanostatic deposition of platinum film: 6 µA, 150 seconds

Figure 31 shows another result of galvanostatic mode deposition where the platinum film is shown to have deposited outside of the contact opening. The bottom layer of the platinum film exhibits the platinum growth around the PS bead template although some regions are flat. During the electrochemistry process, gas bubbles are believed to accumulate under the PS beads and mid-electroplating, the bubble accumulation causes the template to break apart. The electroplating is seen to have continued despite the breakage as bubble-like platinum is observed on the polyimide surface. Only 1 of 5 substrates had unexploded platinum electrodeposition whereas the remaining 4 substrates had burst during electrodeposition.

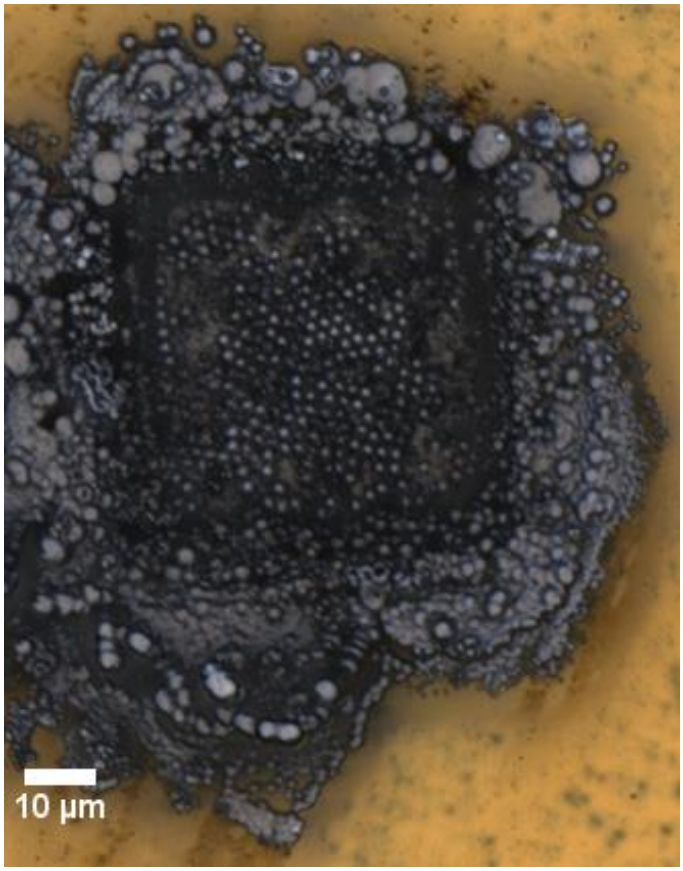

Figure 31. The polystyrene template is believed to have exploded during galvanostatic deposition (6 µA, 150 seconds) of platinum film. The platinum seems to have continued to electroplate despite the breakage of the template. Gas bubble formed during electroplating is believed to have nucleated within the template to cause the breakage

3.3.2.2 Potentiostatic mode electroplating

Figure 32 shows the deposition of platinum film using potentiostatic mode. The working electrode was set at -1.0 V and the deposition time was 150 seconds. The templated platinum is more evenly electroplated than films deposited using current mode. However, the same exploding features were observed in 3 of 5 substrates.

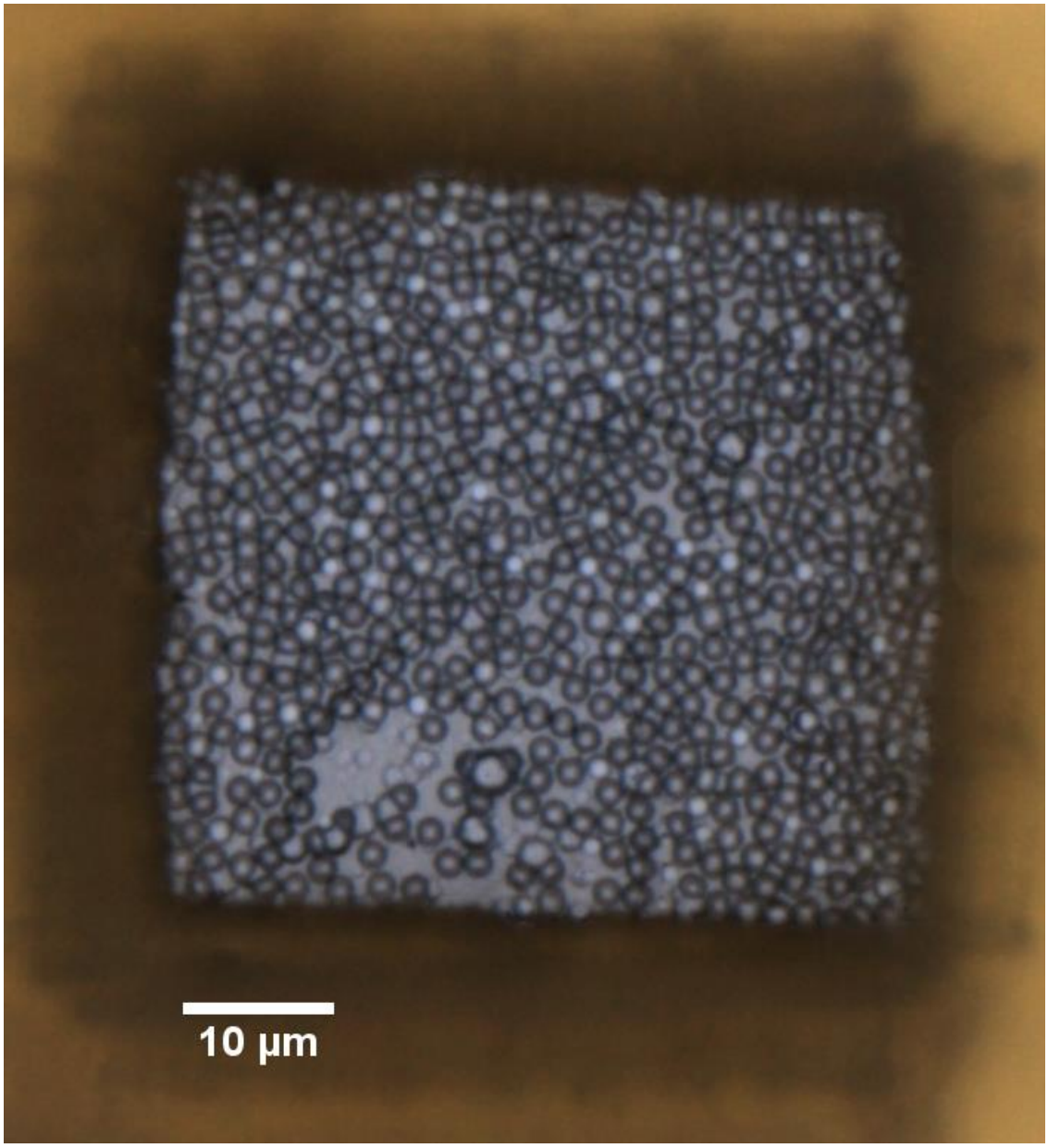

Figure 32. Potentiostatic mode deposition of platinum: -1.0 V, 150 seconds deposition

3.3.2.3 Pulsed-potentiostatic mode electroplating

Figure 33 shows the platinum deposited using pulsed-potentiostatic mode. The working electrode was set to -0.9 V with a 33% duty cycle (15 second period) for 80 pulses altogether. All 5 substrates had even deposition of platinum films and none of the substrates had burst during

electroplating. In the figure, the darker circles are the bottom layer spheres and the brighter circles are the second layer of spheres. When imaged from above, the bottom layer spherical cap will not reflect back some of the incident light due to the skeletal network of platinum whereas an open spherical cap will reflect back all the incident light and will look like a brighter circle.

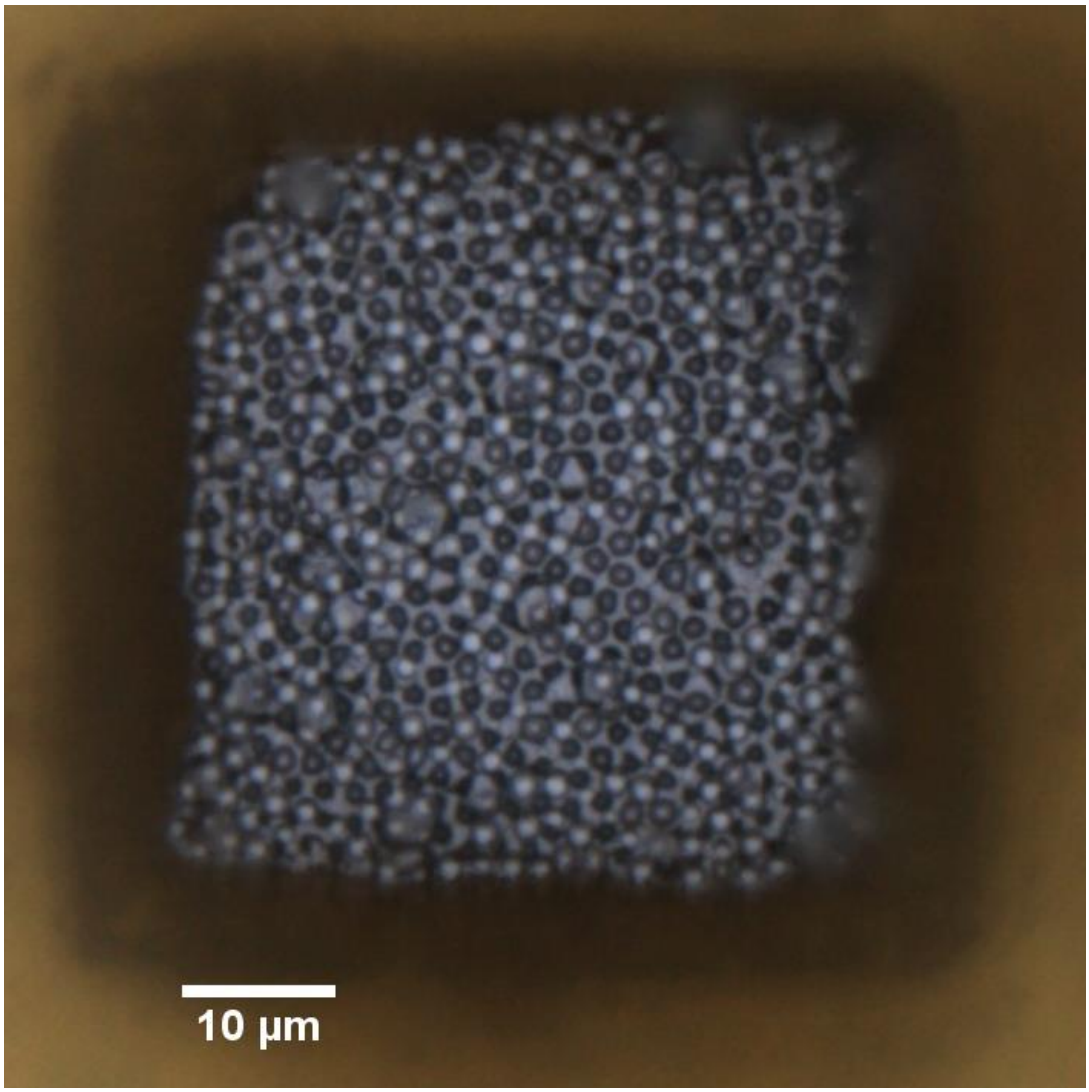

Figure 33. Pulsed-potentiostatic mode electroplating of platinum film: -0.9 V, 80 pulses, [5, 10] sec modulation. The top spherical cap of the first layer of spheres are observed to be darker and the bottom spherical cap of the second layer of bead is brighter when imaged from above

3.3.3 Impedance characteristics of electroplated electrode

The 1 kHz impedance value of unmodified electrode is 1.53 ± 0.172 MΩ (N=5) and the platinum modified impedance is 29.41 ± 3.104 KΩ (N=5). On average, the macroporous platinum film decreased the impedance by an order of 52x. The complex impedance measurement of a platinum modified substrate is shown in Figure 35 and Figure 35. The measured capacitance of plain and macroporous electrode is shown in Figure 36 and the improvement in capacitance (and in effect the surface area) is plotted as a function of frequency in Figure 37. The macroporous Pt film increases the capacitance of the electrode by a factor of 50x at 1 kHz.

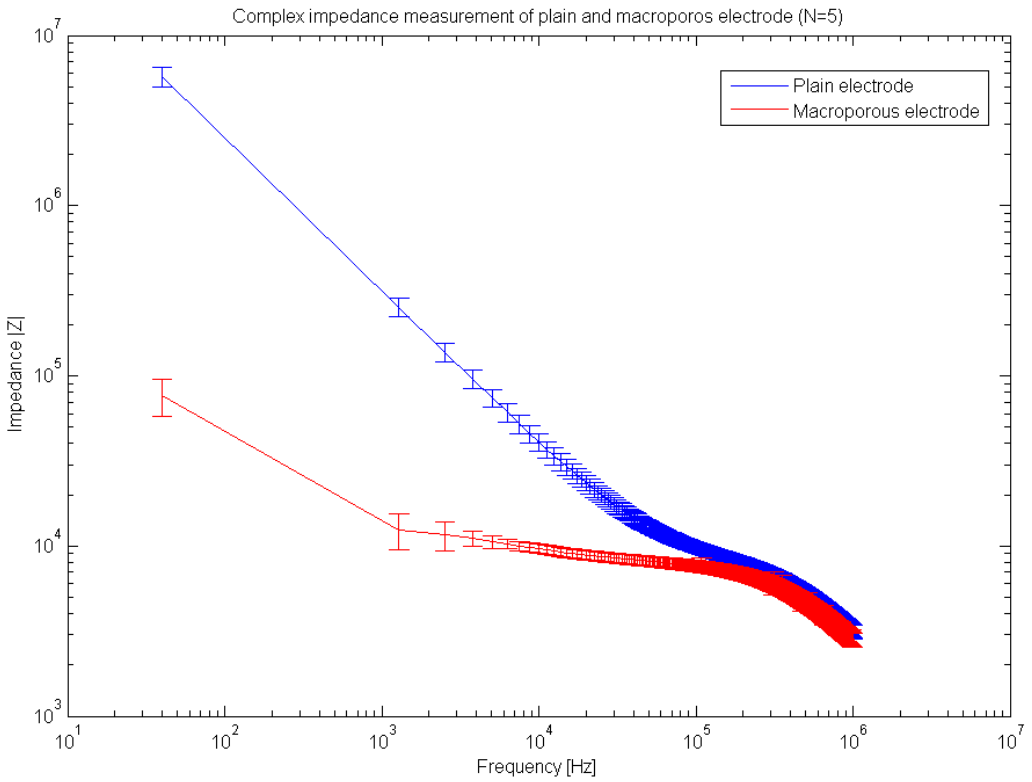

Figure 34. Impedance measurement of plain and macroporous electrode. The 1 kHz impedance decreased by an order 52x

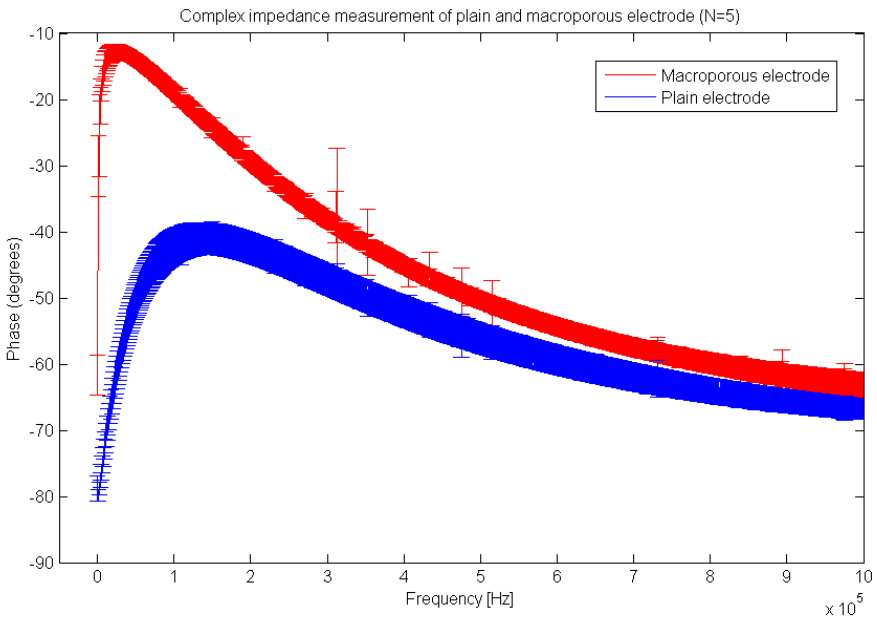

Figure 35. Phase measurement of plain and macroporous electrode

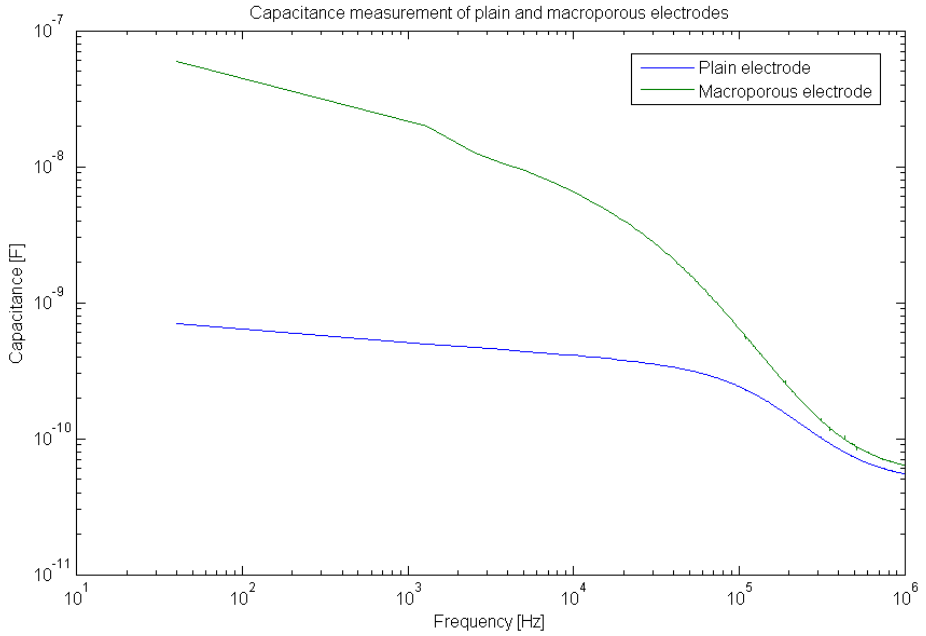

Figure 36. Measured capacitance of plain and macroporous electrode. The macroporous Pt film results in increase in capacitance of the electrode and therefore the effective surface area

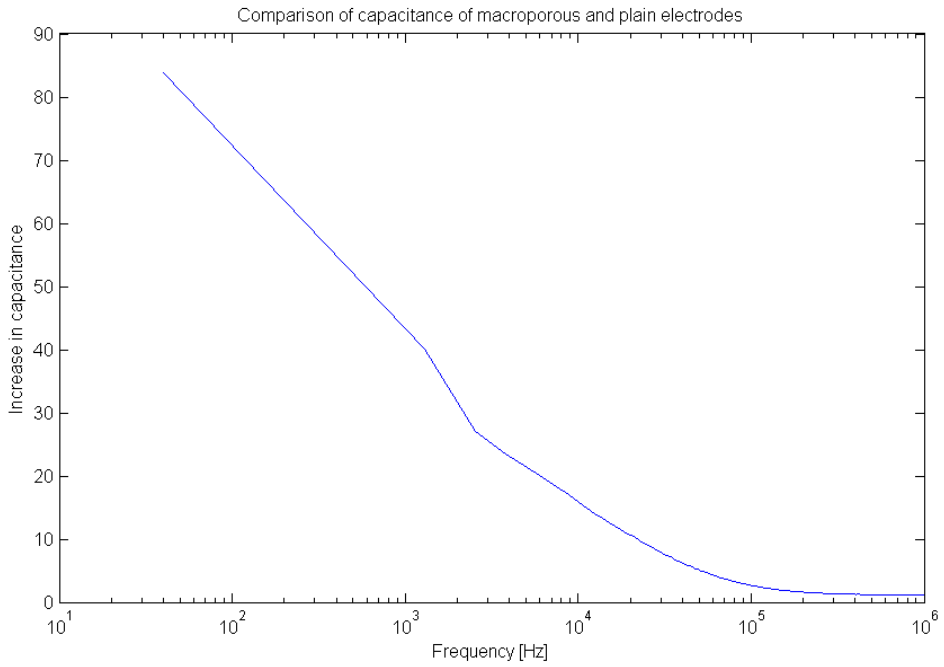

Figure 37. Comparison of measured capacitance for macroporous electrode with respect to plain electrode. The increase in capacitance is high as 80x at 40 Hz and decreases as frequency increases. The capacitance increase at 1 kHz is approximately 50x

The thickness of the flat platinum sections is measured with respect to the exposed gold layer. On average, pulsed-potentiostatic electroplating (-0.9V, 80 pulses 33% duty cycle, 15 second period) results in growing platinum with a thickness of 2.337 ± 0.165 µm (N=5).

3.3.4 Surface area measurement of macroporous platinum film

The numbers of beads were counted, as shown in Figure 38, for each substrate and the surface area contribution from each sphere is estimated using area of spherical cap equation from Section 2.3.4. The height of the spherical cap is determined by measured thickness value of 2.337 ± 0.165 µm (N=5), which indicates all measured diameters of the spheres are on the upper plane of

the center of the sphere. Macroporous platinum modification of microelectrodes increased the surface area by a factor of 1.59 ± 0.054 (N=5) compared to flat unmodified electrode. Approximately 396 ± 7.4 beads were confined in the 50 x 50 µm area.

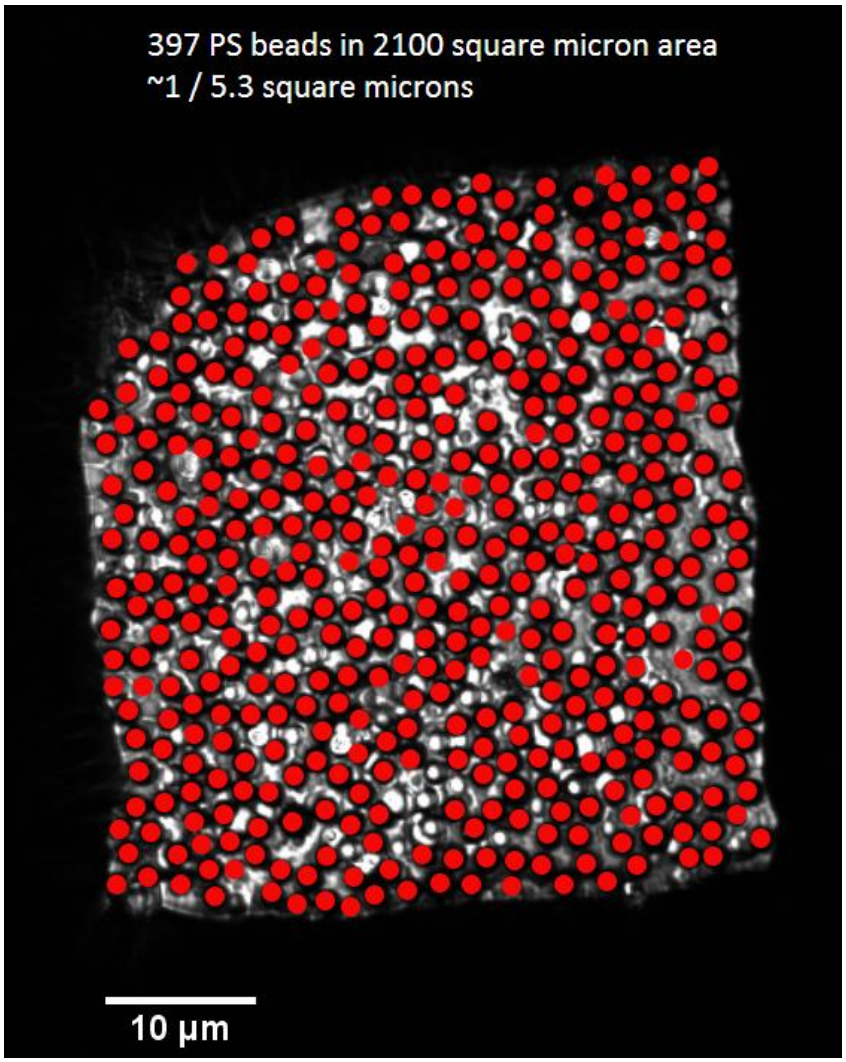

Figure 38. Surface area measurement using image analysis. Each sphere is counted to calculate the surface area contribution from the spherical cap to determine the total surface improvement over unmodified flat electrodes

3.3.5 Polystyrene packing density in hexagonal bounded area

The bead packing density in square bound area was 5.4 ± 0.237 μm^2 per 1 bead (N=5) and the packing density in hexagon bound area was 4.8 ± 0.195 μm^2 per 1 bead (N=5). The hexagon bounded area packs slightly more dense than the square bound area. Figure 39 shows one of the hexagon bound contact opening with 594 counted beads.

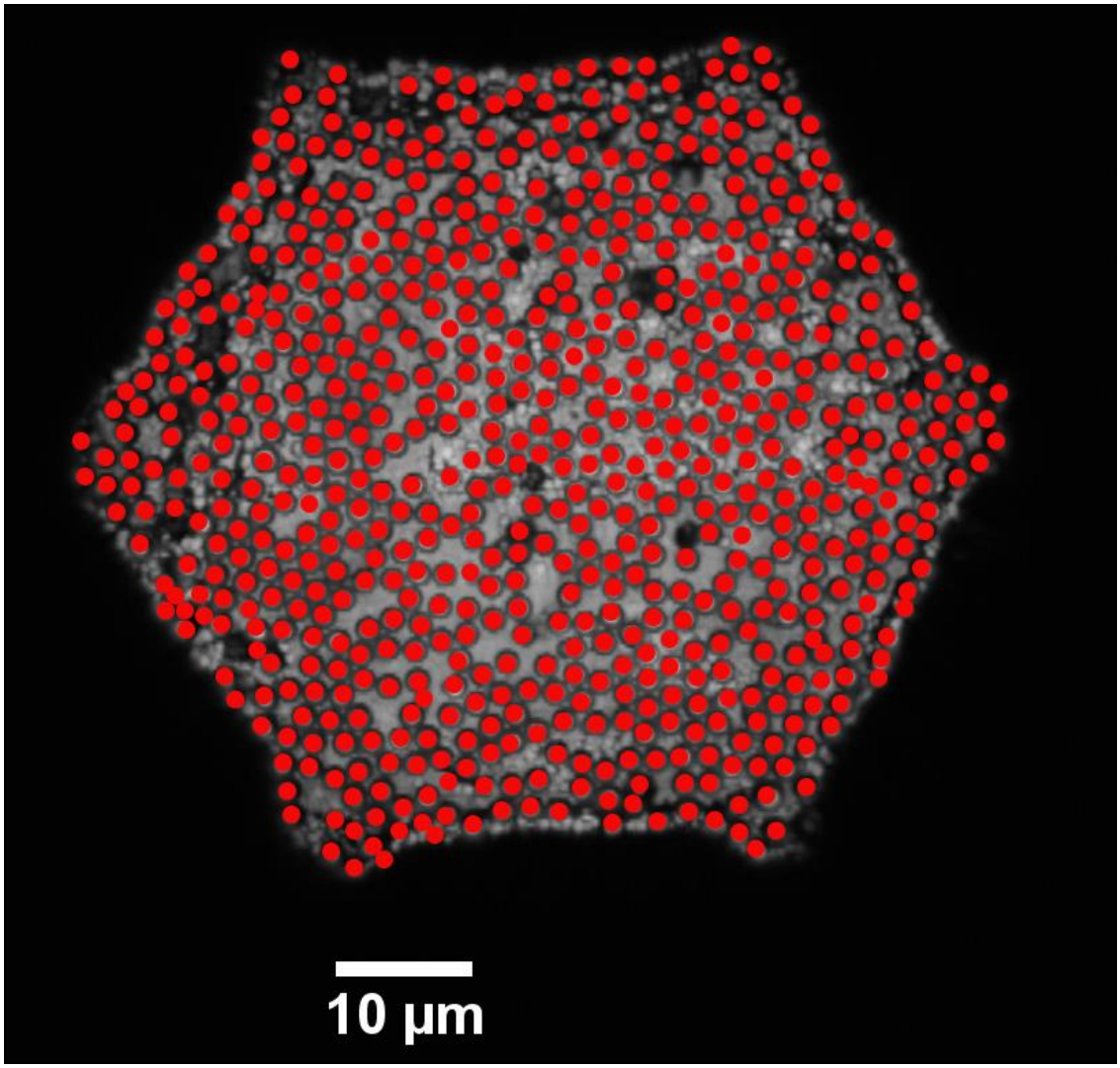

Figure 39. Surface area measurement of hexagon bound contact opening using image analysis. Each sphere is counted to calculate the surface area contribution from the spherical cap to determine the total surface improvement over unmodified flat electrodes

Complete electrochemical depositions of platinum using 0.7 µm polystyrene were unsuccessful. Partial electroplating was possible with contact openings with areas of no polystyrene, as shown in Figure 40. Although inconclusive, in areas where there were polystyrene beads, the ordering of the polystyrene beads does seem to be more ordered than the templates deposited with 2 µm polystyrene beads.

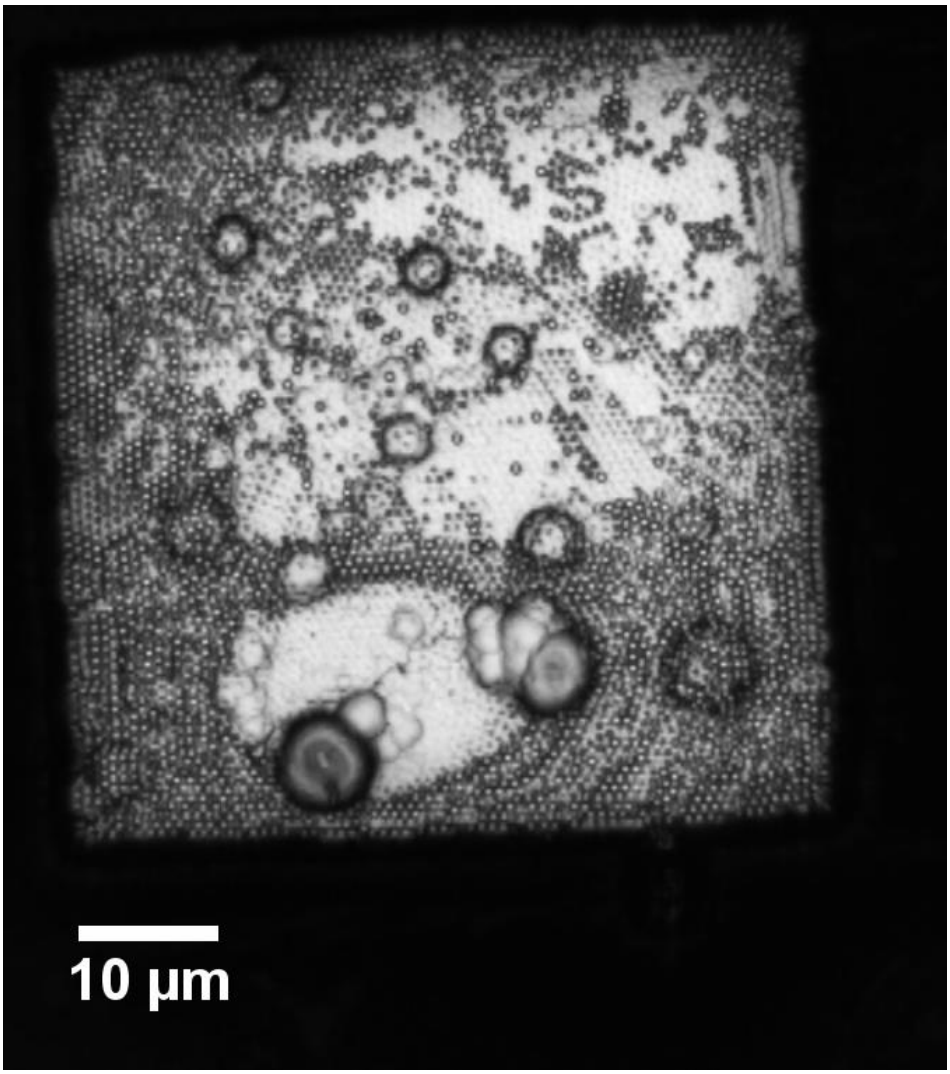

Figure 40. Platinum film deposition using pulsed-potentiostatic mode with 0.7 µm PS bead template. In areas where there no polystyrene, bulbous platinum feature is deposited instead of templated film

Chapter 4: Discussion

4.1 Laser ablation

Laser ablation was successfully used for selective ablation of gold in gold/polyimide substrate as well as polyimide in gold/polyimide and polyimide/gold/polyimide substrates. UV Green (355 nm) laser was optimal in removal of gold without damaging the insulating polyimide layer. For selective removal of polyimide, the laser parameters depend on the substrate layout since the laser absorbance changes with different layout configurations. Selective laser ablation of polyimide in gold/polyimide substrate, common substrate layout in studies exploring selective ablation of polyimide, can be achieved by using UV3 (355 nm) laser with output power of 30% and 20 shots of UV3 (HI) with 15% output power, both at 50 x 50 µm square apertures with 40 Hz frequency. For selective ablation of polyimide for creation of contact openings in a multielectrode array, the bulk of the top layer of polyimide was removed using UV3 (355 nm) laser and a remaining thin membrane of polyimide was removed using lower energy UV3 laser at smaller laser beam size.

The laser beam spot size test results indicate that decreasing the beam spot size while maintaining the same laser output does not damage to the gold layer during selective ablation of polyimide. An output power of 50% with larger laser beam size results in ablation damage to the gold layer while the same output power with small beam size does not damage the gold. The laser beam spot size-induced damage could be due to non-uniform beam intensity on outer edge of the beam profile of the laser. A schematic of a typical pulsed laser system with a mechanical shutter used for setting the laser beam size is shown Figure 41. In the image, the mechanical shutter modulates the size of the laser beam after the beam is focused through the objective

lense. Therefore the shutter can act as an extra filter when blocking out parts of the laser beam while reducing the laser spot size. While the beam profile for the Quik Laze laser system is not available, other experiments studying beam profiles of pulsed ND: YAG laser show that the beam profile can be non-ideal and dependent on generation methods [43].

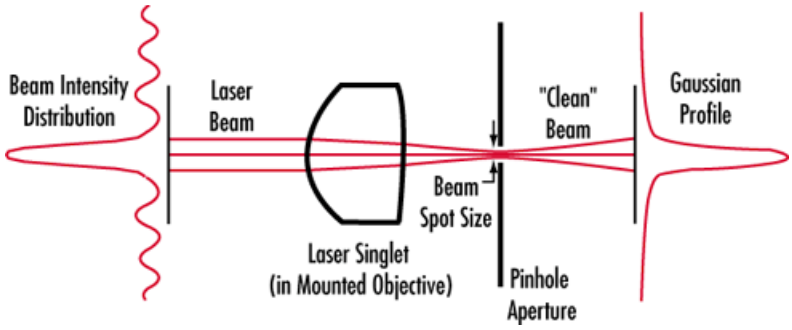

Figure 41. Schematic of a laser ablation system. The pinhole aperture is used to control the beam spot size.

The mechanism for the ablation damage could be due to melting of the gold layer by the incident heat flux from the laser. A finite element modeling of heat conduction in polyimide-gold-silicon substrate by Gabran et al [35] show that most of the heat flux is contained within the gold and silicon whereas the polyimide acts as a thermal insulator. The ablation damage to the gold layer, shown in Figure 19, was consistent with thermal damage characteristics such as surface ripple due to shockwave, and cracks. Thermal properties of gold and polyimide are listed in Table 2.

Table 2. Thermal properties of polyimide and gold

	Thermal conductivity (W/m K)	Heat capacity (J/g K)
gold	320	12.9
polyimide	0.12	109

In summary, laser ablation is an efficient maskless fabrication method for creating contact openings in microelectrode arrays. It is also an efficient method for rapid prototyping of single instances of electrodes. The disadvantages of laser ablation method are that it is a slow, serial process for electrode definition and aligning features across multiple layers is difficult than photolithographic processes due to lack of specialized aligning features with the Quik Laze system.

4.2 Modification of microelectrodes with macroporous platinum film using polystyrene latex sphere template

Laser ablated contact openings were successfully electrochemically deposited with macroporous platinum film using 2 µm diameter non cross-linked polystyrene latex sphere template. Pulsed-potentiostatic mode electrochemical deposition of macroporous platinum increased the effective surface area of the electrodes by an order of 50x at 1 kHz while the macro-geometric surface area of the contact openings were increased by a factor of 1.5x. The 1 kHz impedance was decreased by a factor of 50x.

Polymer brush coating of microelectrodes increases the 1 kHz impedance by a factor of 2.55x. More experiments are required to investigate whether macroporous platinum film modification can offset the impedance change due to polymer brush coating.

The packing order of the 2 µm diameter polystyrene template in a bounded contact opening was not dependent on the drying conditions of the polystyrene solution or the shape of the bound area. Polystyrene templates formed in ambient room setting and saturated humidity environment

were both indistinguishable from each other. Packing densities of templates formed in square and hexagon bound areas were comparably similar to each other as well. Previous experimental results by Bartlett et al. [31] show highly-ordered macroporous platinum films. However, in their experimental setup, the substrate is flat surface area that is 25 times the 50 x 50 µm square contact opening used in this setup . Therefore, the highly ordered polystyrene template is a result of slow evaporation of a larger volume of 300 µL of 0.5 wt % polystyrene solution over a flat surface compared to the 0.1 µL of 2.6 wt % polystyrene solution pipetted over a 10 µm deep 50 x 50 µm square contact opening in this setup.

The polystyrene beads in this experiment are effectively constrained by the 10 µm thick polyimide walls of the contact opening which possibly inhibit self-assembly of the beads during short evaporation period of the 0.1 µL solution. In a more recent study by the same investigators [32], a 12 µm diameter circle electrode was fabricated to study the effect of macroporous platinum film on impedance and noise-level of microelectrodes. The macroporous template was synthesized using 420 nm diameter silica bead template with a Langmuir-Blodgett technique. The packing order of their platinum film deposition (Figure 2, [32]) is similar to packing order of the macroporous platinum film achieved in this experiment, which further support the idea that it is difficult to obtain highly ordered sphere template with a small substrate.

Electroplating of platinum film using 0.7 µm diameter polystyrene bead template was unsuccessful. The smaller sized polystyrene beads completely passivated the contact opening, blocking the current flow during the electrochemistry. Attempt to electroplate using higher voltage was also unsuccessful. Poor diffusion of chloroplatinic solution into the smaller latex

spheres template could be the reason. Minimizing the concentration of polystyrene beads within the contact opening in future experiments could aid with diffusion of the chloroplatinic solution into the polystyrene template. Inkjet printing of polystyrene solution could be the mechanism for minimizing the concentration of beads. However, as previously mentioned, it is difficult to align the tip of the inkjet printer with the contact opening site with the current setup. A solution could be a motorized stage that can be carefully controlled to align the inkjet printer with the substrate.

Flexible microelectrode contact openings were modified with highly reproducible macroporous platinum films using novel fabrication methods. The polystyrene latex template can be deposited using a simple laboratory pipette and evaporated in an ambient room setting. The novelty of the electrochemistry setup allows for macroporous modification of any existing microelectrode array. The electrochemical deposition can be done with a simple pulse-width modulation circuit and a voltage source. The micro-size features of the platinum film allows for further biocompatible polymer brush coating while increasing the electrochemically active surface area of the electrode.

4.3 Future work

In future experiments, microelectrodes modified with macroporous platinum film and polymer brush coating can be studied to observe the overall impedance characteristics. In theory, the improvement in impedance characteristics attributed to platinum films can offset the impedance increase caused by polymer brush coating. A study investigating the brain tissue response to chronic application of macroporous platinum/polymer brush coated electrode can determine the feasibility of using such electrodes for neural devices.

Although inconclusive, initial experiments using smaller diameter polystyrene beads for template formation does hint at the possibility of achieving a more crystalline-like bead structure. The packing order of the template may depend on the ratio of the sphere diameter with respect to the area of the confined contact opening. Therefore, more experiments exploring the relation between the two parameters may further improve the reproducibility of the template structure. An improved inkjet printing setup can aid in modulation of the bead solution for such experiments along with modulated environmental parameters.

The novelty of the electrochemistry method can be further simplified by conducting electrochemical deposition of macroporous structure using simple pulse-width modulation circuitry. The template process can also be tested on already-existing MEAs as well.

Chapter 5: Conclusion

In conclusion, successful laser ablation of materials for rapid prototyping of polyimide-based flexible microelectrodes was carried out. Parameters for selective removal of gold and polyimide in three possible substrate layouts were defined: removal of gold from gold/polyimide, removal of polyimide from polyimide/gold/polyimide substrate, and removal of polyimide from polyimide/gold substrate.

Novel method of depositing macroporous platinum film using latex polystyrene sphere template was presented. The polystyrene bead template is deposited using simple laboratory pipette and the electrochemistry setup was a simplified two-electrode setup. Pulsed-potentiostatic mode deposition of platinum provided even, amorphous-like ordered platinum film. The macroporous platinum film increased the surface area of the electrode contact area by a factor of 50x while decreasing the impedance by two orders of magnitude. Simple image analysis method was used to approximate the surface area increase since conventional hydrogen underpotential method could not be used.

The methods presented in this work can lead to simple methods for making highly desired modifications in biocompatible microelectrodes. Deeper understanding of basic neural systems requires expansive neural information extracted from long-term implantation of microelectrodes.

Bibliography

[1] Nicolelis, M. A. L., D. Dimitrov, et al. (2003). "Chronic, multisite, multielectrode recordings in macaque monkeys." PNAS 100(19): 11041-11046.

[2] Motta, P. S. and J. W. Judy (2005). "Multielectrode microprobes for deep-brain stimulation fabricated with a customizable 3-D electroplating process." IEEE Transactions on Biomedical Engineering 52(5): 923-933.

[3] Burmeister, J. J., F. Pomerleau, et al. (2002). "Improved ceramic-based multisite microelectrode for rapid measurements of L-glutamate in the CNS." Journal of Neuroscience Methods 119(2): 163-171.

[4] Stieglitz, T., H. H. Ruf, et al. (2002). "A biohybrid system to interface peripheral nerves after traumatic lesions: design of a high channel sieve electrode." Biosensors and Bioelectronics 17(8): 685-696.

[5] Stieglitz, T., H. Beutel, et al. (2000). "Micromachined, Polyimide-Based Devices for Flexible Neural Interfaces." Biomedical Microdevices 2(14): 283-294.

[6] Metz, S., R. Holzer, et al. (2001). "Polyimide-based microfluidic devices." Lab on a Chip 1(1): 29-34.

[7] Takeuchi, S., D. Ziegler, et al. (2005). "Parylene flexible neural probes integrated with microfluidic channels." Lab on a Chip 5: 519-523.

[8] Wise, K. D. (2005). "Silicon microsystems for neuroscience and neural prostheses." Engineering in Medicine and Biology Magazine, IEEE 24(5): 22-29.

[9] Liu, X., D. B. McCreery, et al. (1999). "Stability of the interface between neural tissue and chronically implanted intracortical microelectrodes." IEEE Transactions on Rehabilitation Engineering 7(3): 315-326.

[10] Kovacs, G. T. A. (1994). Introduction to the Theory, Design, and Modeling of Thin-Film Microelectrodes for Neural Interfaces. Enabling Technologies for Cultured Neural Networks. D. A. Stenger and T. M. McKenna, Academic Press: 121-165.

[11] Perlmutter, Joel S., and Jonathan W. Mink. "Deep brain stimulation." Annu. Rev. Neurosci. 29 (2006): 229-257.

[12] "Cochlear Implants." *National Institute on Deafness and Other Communication Disorders*. N.p., n.d. Web.

[13] Margalit, Eyal, et al. "Retinal prosthesis for the blind." Survey of ophthalmology47.4 (2002): 335-356.

[14] Schwarz, David A., et al. "Chronic, wireless recordings of large-scale brain activity in freely moving rhesus monkeys." Nature methods (2014).

[15] Wise, K. D. (2005). "Silicon microsystems for neuroscience and neural prostheses." Engineering in Medicine and Biology Magazine, IEEE 24(5): 22-29.

[16] Kandel, Eric R., James H. Schwartz, and Thomas M. Jessell, eds. Principles of neural science. Vol. 4. New York: McGraw-Hill, 2000.

[17] Strumwasser, F. (1958). "Long-Term Recording from Single Neurons in Brain of Unrestrained Mammals." Science 127(3296): 469-470.

[18] Lebedev, Mikhail A., et al. "Future developments in brain-machine interface research." Clinics 66 (2011): 25-32.

[19] Wise, Kensall D., James B. Angell, and Arnold Starr. "An integrated-circuit approach to extracellular microelectrodes." Biomedical Engineering, IEEE Transactions on 3 (1970): 238-247.

[20] Cheung, Karen C., et al. "Flexible polyimide microelectrode array for in vivo recordings and current source density analysis." Biosensors and Bioelectronics22.8 (2007): 1783-1790.

[21] D. H. Szarowski, M. D. Andersen, S. Retterer, A. J. Spence, M. Isaacson, H. G. Craighead, J. N. Turner, and W. Shain. Brain responses to micromachined silicon devices. Brain Res, 983(1-2):23–35, Sep 2003.

[22] Stieglitz, Thomas, et al. "Flexible, polyimide-based neural interfaces."*Microelectronics for Neural, Fuzzy and Bio-Inspired Systems, 1999. MicroNeuro'99. Proceedings of the Seventh International Conference on*. IEEE, 1999.

[23] Karen C. Cheung. Implantable microscale neural interfaces. Biomed Microdevices, 9(6):923–938, Dec 2007.

[24] Roy Biran, David C. Martin, and Patrick A. Tresco. Neuronal cell loss accompanies the brain tissue response to chronically implanted silicon microelectrode arrays. Exp Neurol, 195(1):115–126, Sep 2005.

[25] Polikov, Vadim S., Patrick A. Tresco, and William M. Reichert. "Response of brain tissue to chronically implanted neural electrodes." *Journal of neuroscience methods* 148.1 (2005): 1-18.

[26] THIEBAUD, P. 1999. Fabrication of microelectrode arrays for electrophysiological monitoring of hippocampal organotypic slice cultures by interface. PhD, University of Neuchatel.

[27] Beebe, X. & Rose, T. L. 1988. Charge injection limits of activated iridium oxide electrodes with 0.2 msec pulses in bicarbonate buffered saline. IEEE Transactions on Biomedical Engineering, 35, 494-495.

[28] Gabay, T., Ben-David, M., Kalifa, I., Sorkin, R., Abrams, Z. E. R., Ben-Jacob, E. & Hanein, Y. 2007. Electro-chemical and biological properties of carbon nanotube based multi-electrode arrays. Nanotechnology, 18, 035201.

[29] Abidian, M. R., Salas, L. G., Yazdan-Shahmorad, A., Marzullo, T. C., Martin, D. C. & Kipke, D. R. Year. In-vivo Evaluation of Chronically Implanted Neural Microelectrode Arrays Modified with Poly (3,4-ethylenedioxythiophene) Nanotubes. In: SALAS, L. G., ed. Neural Engineering, 2007. CNE '07. 3rd International IEEE/EMBS Conference on, 2007. 61-64.

[30] Gao, Guangzheng, et al. "The biocompatibility and biofilm resistance of implant coatings based on hydrophilic polymer brushes conjugated with antimicrobial peptides." *Biomaterials* 32.16 (2011): 3899-3909.

[31] Bartlett, P. N., et al. "Highly ordered macroporous gold and platinum films formed by electrochemical deposition through templates assembled from submicron diameter monodisperse polystyrene spheres." *Chemistry of Materials* 14.5 (2002): 2199-2208.

[32] Heim, Matthias, et al. "Combined macro-/mesoporous microelectrode arrays for low-noise extracellular recording of neural networks." *Journal of neurophysiology*108.6 (2012): 1793-1803.

[33] Preuss, S., A. Demchuk, and M. Stuke. "Sub-picosecond UV laser ablation of metals." *Applied Physics A* 61.1 (1995): 33-37.

[34] Srinivasan, R., B. Braren, and R. W. Dreyfus. "Ultraviolet laser ablation of polyimide films." *Journal of applied physics* 61.1 (1987): 372-376.

[35] Gabran, S. R. I., R. R. Mansour, and M. M. A. Salama. "Maskless pattern transfer using 355nm laser." *Optics and Lasers in Engineering* 50.5 (2012): 710-716.

[36] Lazare, Sylvain, and Vincent Granier. "Ultraviolet laser photoablation of polymers: a review and recent results." *Laser Chem* 10.1 (1989): 25-40.

[37] Welch, A. J., et al. "Laser thermal ablation." *Photochemistry and photobiology*53.6 (1991): 815-823.

[38] Baddo, Phillipe, Dr., William Clark, Dr., and Ali Said, Dr. "Ultrafast Laser Micromachining Handbook." *Ultrafast Laser Micromachining Handbook*. Clark-MXR, 2011. Web. 14 Aug. 2014.

[39] New Wave Research, “Laser machining of semiconductor, CLD and microelectronic devices.” Technical report, New Wave Research, June, 1998.

[40] Zou, Yuquan, et al. "Barrier capacity of hydrophilic polymer brushes to prevent hydrophobic interactions: Effect of graft density and hydrophilicity."*Macromolecules* 42.13 (2009): 4817-4828.

[41] Cui, Xinyan, and David C. Martin. "Electrochemical deposition and characterization of poly (3, 4-ethylenedioxythiophene) on neural microelectrode arrays." *Sensors and Actuators B: Chemical* 89.1 (2003): 92-102.

[42] Williams, Justin C., et al. "Complex impedance spectroscopy for monitoring tissue responses to inserted neural implants." *Journal of neural engineering* 4.4 (2007): 410.

[43] Tamuri, A.R.et al. “Beam spot of Q-switched ND: YAG laser based on raster graphic.” IJRRAS 4(4) September, 2010.